Universidade do Minho
Escola de Engenharia

Mafalda Araújo Seara Couto

3D Modelling and Design of a Bioloid Compliant Quadruped Leg

Dissertação de Mestrado
Ciclo de Estudos Integrados Conducentes ao
Grau de Mestre em Engenharia Biomédica

Trabalho realizado sob a orientação de
Professor Doutor José Mendes Machado
Professora Doutora Cristina Manuela Peixoto dos Santos

DECLARAÇÃO

Nome: Mafalda Araújo Seara Couto

Endereço electrónico: a49983@alunos.uminho.pt Telefone: +351 916 818 290

Número do Bilhete de Identidade: 13372480

Título dissertação:

3D Modelling and Design of a Bioloid Compliant Quadruped Leg

Orientadores:

Professor Doutor José Mendes Machado

Professora Doutora Cristina Manuela Peixoto dos Santos

Ano de conclusão: 2011

Designação do Mestrado:

Mestrado em Engenharia Biomédica

Área de Especialização: Biomateriais, Reabilitação e Biomecânica

Escola: de Engenharia

Departamento: de Engenharia Mecânica

Nos exemplares das teses de doutoramento ou de mestrado ou de outros trabalhos entregues para prestação de provas públicas nas universidades ou outros estabelecimentos de ensino, e dos quais é obrigatoriamente enviado um exemplar para depósito legal na Biblioteca Nacional e, pelo menos outro para a biblioteca da universidade respectiva, deve constar uma das seguintes declarações:

1. É AUTORIZADA A REPRODUÇÃO INTEGRAL DESTA TESE/TRABALHO APENAS PARA EFEITOS DE INVESTIGAÇÃO, MEDIANTE DECLARAÇÃO ESCRITA DO INTERESSADO, QUE A TAL SE COMPROMETE;

2. É AUTORIZADA A REPRODUÇÃO PARCIAL DESTA TESE/TRABALHO (indicar, caso tal seja necessário, nº máximo de páginas, ilustrações, gráficos, etc.), APENAS PARA EFEITOS DE INVESTIGAÇÃO, , MEDIANTE DECLARAÇÃO ESCRITA DO INTERESSADO, QUE A TAL SE COMPROMETE;

3. DE ACORDO COM A LEGISLAÇÃO EM VIGOR, NÃO É PERMITIDA A REPRODUÇÃO DE QUALQUER PARTE DESTA TESE/TRABALHO

Universidade do Minho, _____/_____/_____

Assinatura: _____

Acknowledgements

To my parents and my brother

First of all, I would like to give special thanks to my supervisor Prof. Dra. Cristina Santos for her professional support, guidance and encouragement throughout the development of this dissertation. I deeply appreciate her many efforts to proofread my dissertation over and over again.

I am extremely grateful to my dissertation co-supervisor, Prof. Dr. José Machado, from the Department of Mechanical Engineering, for all the availability and orientation along the semester which has been fundamental in the elaboration of this project.

To all the researchers from the Robotics Laboratory, with a special thanks to Vitor Matos and Miguel Oliveira, for their extensive knowledge and range of ideas during my work in the Webots™ software.

My greatest acknowledgement goes to my family, my parents and my brother, for all the encouragement and support along the five years as a student. Love and thank for the values, the caring and trust, you are my motivation and my pride.

To my "academic family", with whom I have learn so much, thanks for the happiness, thanks for the brotherhood, thanks for all the sharing moments and finally thanks for the love.

Big thanks to my friends, for the companionship, the joy, the affection, for their never-ending patience, support and encouragement, but mostly for the friendship. You were fundamental during this time. Thanks for listening and accompaning me, thanks for being there.

Finally, my thanks go to all those who are not particularly mentioned here. The work presented could not have been made without the support from many individuals.

Abstract

In the growing fields of rehabilitation robotics, prosthetics, and walking robots, the modeling of a real robot is a complex and passionate challenge. On the crossing point of mechanics, physics and computer-science, the development of a complete model involves multiple tasks ranging from the 3D modeling of the different body parts, the measure of the different physic properties, the understanding of the requirements for an accurate simulation, to the development of a robotic controller.

In order to minimize large forces due to shocks, to safely interact with the user or the environment, and knowing the ability of passive elastic elements to store and release energy, compliant mechanisms are increasingly being applied in robots applications.

This work aims to the elaboration of an accurate efficient three-dimensional model of the legs of the quadruped Bioloid robot and the development of a world showing the effect on Webots™ simulation software developed by Cyberbotics Ltd. The goal was to design a segmented pantographic leg with compliant joints, in order to actively retract the collision and the impact of the quadruped legs with the ground during locomotion. Geometrical and mechanical limits have to be evaluated and considered for the modeling setup.

Finally a controller based on the use of Central Pattern Generators was improved in order to adapt to the novel model and simple tests were performed in the Webots™, rendering a 3D model simulation for the different values of spring-damping coefficients at the legs knee joint. Through the a MATLAB® algorithm, the characterization of the joint angles during simulation was possible to be assessed.

Resumo

A modelação de um robot real é um desafio complexo e fascinante na crescente área da Robótica, que engloba desde robots de reabilitação, próteses a uma diversidade de outros dispositivos locomotores. No cruzamento da mecânica com a física e as ciências computacionais, o desenvolvimento de um modelo completo envolve várias tarefas que vão desde a modelação 3D das diferentes partes do corpo, a medição das propriedades físicos inerentes, a compreensão dos requisitos para uma simulação precisa bem como a aplicação de um controlador robótico.

A fim de minimizar grandes forças devido a choques, interagir com segurança com o utilizador ou o ambiente e conhecendo a capacidade de armazenagem de energia por parte de elementos elásticos passivos, um sistema de amortecimento-mola demonstra ser uma aplicação de crescente interesse na Robótica.

Este trabalho visa a elaboração de um modelo tridimensional eficiente e preciso das pernas do robô quadrúpede Bioloid a ser reproduzido num mundo no software Webots™ desenvolvido pela Cyberbotics Ltd. O objectivo foi desenhar uma perna pantográfica segmentada tridimensional a ser aplicada em paralelo com um sistema de amortecimento-mola de forma a retrair activamente a colisão e o impacto das patas do quadrúpede com o solo durante a locomoção. Deste modo para uma configuração do modelo bem sucedida são tidos em conta limites geométricos e mecânicos.

Por ultimo, o controlador com base no uso de 'Central Pattern Generators' foi melhorado a fim de se adaptar ao novo modelo e por conseguinte foram realizados testes simples usando o simulador Webots™. Nesta parte experimental é realizada a simulação do modelo permitindo avaliar o comportamento do modelo 3D para diferentes valores de coeficientes de mola e de amortecimento aplicados a nível do joelho da perna. Através de um algoritmo MATLAB® é possível caracterizar e analisar o comportamento doa ângulos das juntas durante a simulação.

Table of Contents

Abbreviations and Acronyms

DoF	Degrees of Freedom
ODE	Open Dynamics Engine
CoM	Center of Mass
CPG	Central Pattern Generator
SEA	Series Elastic Actuator
MACCEPA	Mechanically Adjustable Compliance and Controllable Equilibrium Position Actuator
PAM	Pneumatic Artificial Muscles
PPAM	Pleated Pneumatic Artificial Muscles
VSA	Variable Stiffness Actuator
AMASC	Actuator with Mechanically Adjustable Series Compliance
VSSEA	Variable Stiffness Series Elastic Actuator
$\boldsymbol{\lambda_1}$	normalized length of the first leg segment (thigh/scapula)
$\boldsymbol{\lambda_2}$	normalized length of the second leg segment (shank/upper arm)
$\boldsymbol{\lambda_3}$	normalized length of the third leg segment (foot/lower arm)
$\boldsymbol{\lambda_p}$	normalized distance of the pantograph attachment l_2 to l_4,
$\boldsymbol{l_1}$	absolute length of the first leg segment (thigh/scapula)
$\boldsymbol{l_2}$	absolute length of the second leg segment (shank/upper arm), l_4
$\boldsymbol{l_3}$	absolute length of the third leg segment (foot/lower arm)
$\boldsymbol{l_p}$	absolute length of the pantograph l_2 to l_4 attachment, $\lvert CD\rvert = \lvert EF\rvert$

$\boldsymbol{k_{leg}}$	leg stiffness of the virtual leg
$\boldsymbol{m}$	body mass
$\boldsymbol{g}$	gravitational acceleration: 9.81 m/s²
$\boldsymbol{\varphi}$	leg angle between $l_1/l_{2,4}$ or $l_3/l_{2,4}$
$\boldsymbol{L_T}$	fully extended total length of the leg: 0.21 m
$\boldsymbol{L_0}$	length of the leg at touchdown
$\boldsymbol{L}$	current leg length
$\boldsymbol{l_\lambda}$	relative leg length
$\boldsymbol{\alpha_{leg}}$	angle between the leg segment and the virtual leg
$\boldsymbol{\beta}$	angle of attack of the virtual leg
$\boldsymbol{F_{leg}}$	leg force
$\boldsymbol{v_{x,y}}$	velocity of the center of mass with respect to the coordination system
$\boldsymbol{t_c}$	time of contact
$\boldsymbol{\theta}$	half-angle of the virtual leg
$\boldsymbol{k, k_{spring}}$	spring constant at the knee joint
$\boldsymbol{c, c_{damping}}$	damping constant at the knee joint

List of Figures

List of Tables

1 Introduction

This chapter presents the context of the framework, defining objectives to the development, as well as the motivations of the global project. This section ends with a brief description of the dissertations structure.

1.1 The work presentation and motivation

The work developed in the present dissertation had the duration of one semester, being developed in the Control, Automation and Robotics Group of the University of Minho, in Guimarães.

Nowadays, Robotics is growing fast and in the most fields, making a significant impact on many aspects of modern life. Locomotive robots are no exception and became an attractive field of research. Walking machines have a major interest in a large range of applications, from industry to healthcare, transportation, military applications, space and sea exploration, providing many advantages over human faculties in many of these situations in terms of safety and effectiveness [1] [2] [3].

Currently, the biomechanical models are very complex and their application in modeling keeps being applied on several areas. In robotics there are several studies and projects

mimicking the human and animal behavior to improve the knowledge about their mechanisms and ultimately succeed in the many significant fields, like rehabilitation.

The modeling and design of a robot is a complex and interesting challenge, therefore in order to minimize large forces due to shocks and to safely interact with the user or the environment, the motivation of this work aims to the elaboration of an accurate efficient three-dimensional model of a quadruped robot with compliant legs.

The main goal of this project is to improve the leg design of the Bioloid quadruped robot, from a three-dimensional model developed by Fillion-Robin [4]. For this purpose a new segmented pantographic robotic leg design was created using the Webots™ simulation software, with passive compliant knee joints associated.

Focusing on a main issue which is the leg retraction, the design features to be implemented are essential for the performance of the quadruped when it contacts the ground. Thus, the use of well-designed passive compliant system comes as a benefit in order to obtain a successful operative leg. This component is not only useful to store energy and reducing power consumption, it also helps to make a segmented leg safe and robust when faced with external perturbations [5].

This project aim to a final leg incorporated in the Bioloid quadruped robot in order to perform a stable and linear locomotion. With the goal of a future real assembling of the developed mechanism the objective was to achieve a stable simulation of the novel quadruped using a qualified virtual software.

1.2 Bioloid robot presentation

The ROBOTIS® is a well-known, specialized company developer of robotic kits with a wide set of advantageous features, thus it holds an academic interest on research in many fields, greatly due to its robustness and versatility. The kit used in this project is named BIOLOID. Figure 1.1 illustrates the dog assembly known as “Puppy”.

Figure 1.1 - Puppy BIOLOID robot [6].

The basis of this project was the model created by Fillion-Robin [4], which holds a three-dimensional model that closely resembles a real dog robot, as illustrated in Figure 1.2. Therefore some of the main characteristics (orientations, weight, etc.) presented in the Webots™ world from [4] were maintained.

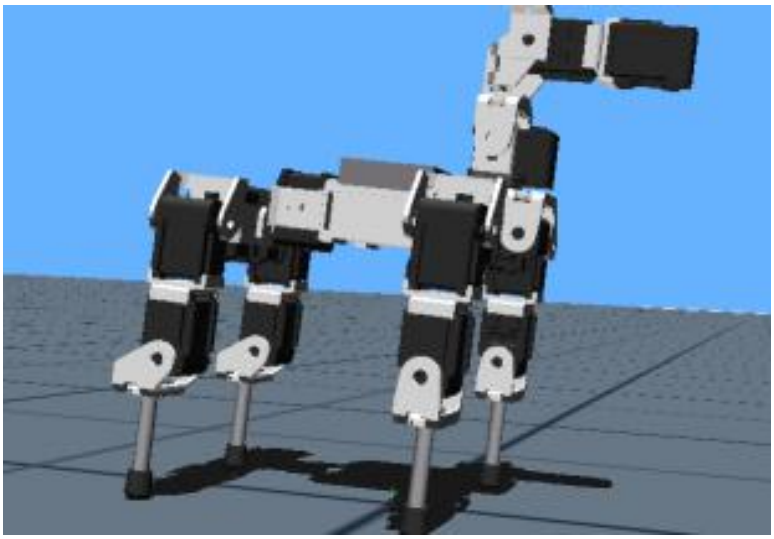

Figure 1.2 - Quadruped robot model rendered in Webots™ [4].

The robot design aim for the development of an accurate leg model both efficient and robust for a quadruped, using the same Webots™ simulator software to the rendering of a 3D model. The Webots™ platform, developed by Cyberbotics Ltd, in collaboration with the Swiss Federal Institute of Technology in Lausanne, performs a rapid prototyping environment for modeling, programming and simulating mobile robots models, demonstrating the different phases of the reproduction of the motion [4].

Webots™ reproduces several accurate properties, very important for modeling such as shape, color, mass, friction or density. The core of this software is based on the robust and powerful physics engine: Open Dynamics Engine (ODE). The two main components of ODE are the rigid body dynamics simulation engine and the collision detection engine, known to be a successful and promising Physics tool, working as a library to provide more realistic simulations [4].

The Bioloid kit used is composed of a collection of mechanically indispensable components to robots performance: high density plastic block-shaped parts which are responsible for the interconnection of the elements providing the apparatus cohesion during motion; an actuation controller, the CM5 processor unit; and for the articulations actuation, the Dynamixel AX-12 servomotors.

These units can be assembled together in a single system, however the interactivity of these components with each other carries a considerable level of complexity [4] [7] [8]. The servomotors are chained in a hierarchical series configuration and to control these servo components there is an actuation unit which can be programmed via a supplied program named CodeBlocks. This program is an Integrated Development Environment software that is responsible for the motion generation of the model [9].

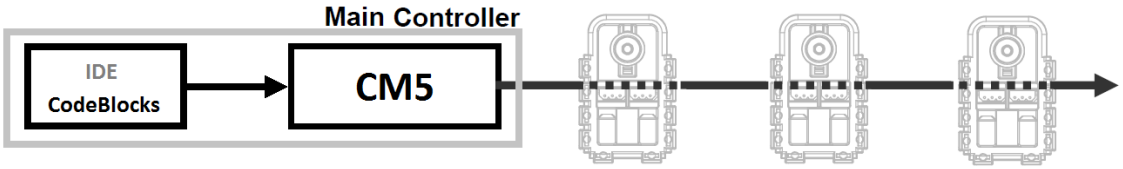

Figure 1.3 – Control process and disposition block diagram for Bioloid motion generation [6].

1.3 Considerations of the model

Despite the good characteristics of the former model, several aspects can be improved. In order for a robotic device to be successful in a known application, it needs to interact safely and efficiently with its user or the environment [4] [10].

As mentioned, from the previous Bioloid quadruped configuration model, some main characteristics were maintained. First of all, the leg presents same degrees of freedom (DoF), where each leg is able to move in three axes: hip joint can be actuated for pitch and roll and the knee joint that is also actuated for the pitch angle variation, thereby the motion generation takes place only for the sagittal plane. While the hip active joint main actuation is responsible for the protraction and retraction of the leg holding the locomotion main control, the knee joint has the function of extend and contract the leg. This last mentioned joint also will hold a spring-damp system that is responsible for impact absorption during stance phase of the walking cycle.

Secondly, should be emphasized that the configuration of the leg was only change after the knee joint extension, maintaining the trunk, head and upper parts of the limbs as the original model.

In recent years, there are more and more designed robots, which are biomomimetics copies of animals. Cheetah [11], furthermore named Oncilla, is a robot developed by BioRob (Biologically Inspired Robotics Group) in Switzerland at the École Polytechnique Fédérale De Lausanne (EPFL) that tries to follow this idea. It features complex model of a compliant, pantographic leg with passive dynamics that was designed from observations in small mammals. Taking the Cheetah/Oncilla as an inspiration, the new leg was developed using a pantographic model responsible for the extension and retraction at the knee joint during locomotion.

In the Webots™ world the implementation of the pantographic mechanism introduces a concern in the physics characterization. Thus, the geometrical and mechanical limits regarding the system must be considered in the modeling, in other words, the demanding parallelism condition of the new mechanism must be properly implemented on the physics plug-in in order to obtain an accurate and dynamic simulation.

In addition to these modeling parameters, also the control of the robot will held some configuration setting. The servomotors features will be reproduced as the Dynamixel AX-12 actuation characteristics. Afterwards, the locomotion control of the servos will be carried out by Central Pattern Generators (CPGs). These prove to be a adequate by mimicking the animals in the production of rhythmic neural activity to control their movements, through the generation of

oscillatory signals for the actuators, enabling stable periodic gaits and also the achievement of complex behavior in different kind of environments [5] [12] [13] [14].

1.4 Structure of the dissertation

The first chapter of this dissertation summarizes the main goals of the work, presenting the project theoretical framework and motivations. In this same chapter is also mentioned which are the achieving goals as well as the practical work and considerations to the developing model, finalizing with a description of the dissertation.

Before the modeling and experimentation it was carried out a study on the compliant systems developed by researchers and a state-of-the-art concerning the passive compliant actuators with applications in locomotion mechanisms, developed in the past few years. This part of the dissertation is presented in the second chapter, addressing the analysis and comparison of these systems.

In chapter number three, is presented the leg design developed for legged robots, distinguishing the different types of structures. Focusing on the pantographic configuration benefits in the leg retraction, the Cheetah, also known as Oncilla, quadruped characteristics are deepen analyzed, incorporating the information about the three-segmentation, structural setup and ultimately the considerations of the compliant mechanism.

The forth part of the body of this dissertation approaches the modeling of the new leg. The kinematic analysis of the leg is developed in order to establish limitative parameters for the joints configuration and consequently repercussion in the experimental simulation. Also, the spring-damp coupled system is assessed for the desired retraction.

The practical part of this work is described and analyzed in the fifth chapter, where it is characterized the Webots™ configuration parameters to be introduced in the modeling as well as the physics plug-in of the new mechanism. This chapter addresses the analysis of the controller of the servomotors for the locomotion step cycle. Ultimately the world file model is accomplished and the simulation is carried out. Throughout a MATLAB® algorithm the results were able to be presented and discussed.

Finally in the last chapter, the final statements and conclusions are described and some future work considerations are suggested in order to improve the legs performance in a walking gate with a compliance system.

2 Passive compliant actuation systems

In this chapter it is exploited the study of the principal compliant actuators applied along the years in the different walking robots. Firstly, a state-of-the-art of the compliant actuation technologies is presented as well as the functional principles of each implementation case. Ultimately a brief comparison is done in an effort to distinguish the requirements and features for the different stiffness actuators design.

2.1 State of the art of passive compliant actuators

Research in legged locomotion is evolving and new technologies are being exploited worldwide with the aim of improving actuator performance [10]. Thereby for the rehabilitation robotics, prosthetics, and walking robots, variable stiffness actuators or adjustable compliance actuators design and implementation are being upgraded. Due to their interesting properties regarding safe human-robot interaction, reducing large shock-forces and improving energy-efficient locomotion, they are becoming an inspiration in the Robotics field. The presence of internal elastic elements provides the ability to store and release energy of walking/running robots and prostheses of the passive elastic elements [15] [16] [17] [18] [19].

According to Laffranchi study report on compliant actuators [19], first of all the functional principles can be differentiated by their stiffness characterization, which can be fixed or variable. On the following section is presented a comparison of the mechanical design between the different compliant actuators [17].

2.1.1 Actuators with fixed compliance

Actuators with fixed compliance represent the first attempts towards the development of compliant actuation systems, incorporating in its structure an element with fixed passive stiffness. These systems can be implemented following two main approaches, the antagonistic or the series design [19].

A specific case of a fixed passive spring in series configuration with the actuation system (as electric motors or hydraulic systems) is the *Series Elastic Actuator* (SEA), developed by Williamson in 1995 [10], illustrated in Figure 2.1. These actuators employ only one actuator and one elastic element per degree of freedom [15] [19].

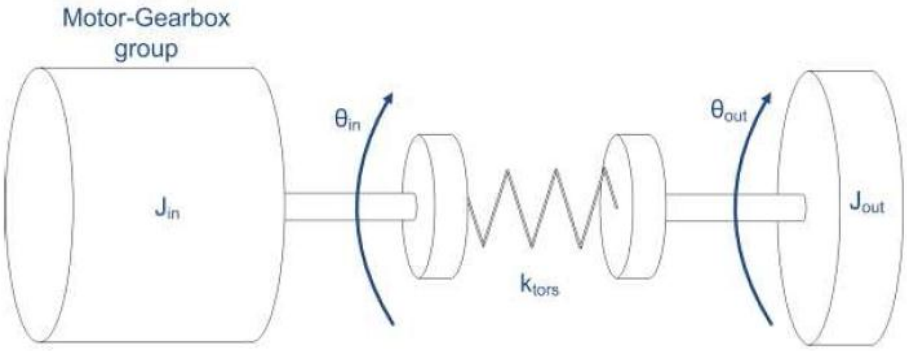

Figure 2.1 - A conceptual schematic of fixed compliance actuator adapted from SEA [19].

The element with the fixed passive stiffness is placed between the rigid actuator and the load. These configurations show equilibrium-controlled stiffness, in other words the equilibrium position of the spring is controlled to exert a desired force or stiffness. The compliance is actively changed when the motor position is adjusted based on the deflection of the spring to alter the tension or compression of the spring, in other words, the motor torque of the actuator is proportional to the displacement of the unit and force on the spring.

To obtain variable stiffness, the virtual stiffness of the actuator is adjusted by dynamically variation of the equilibrium position of the spring. The use of series elastic actuators improve the performance of repetitive motion tasks as walking, exhibiting stable behavior while in contact with all environments [10] [15].

The improvements brought by Series Elastic Actuators, such as safety in human-robot interaction, ability to absorb the shocks and enhancement of the force/torque control performance are also applicable for fixed stiffness antagonistic setups. Actually, an antagonistic joint is made of two series elastic actuators displayed antagonistically which transmits the agonist/antagonist forces to the joint [19].

2.1.2 Actuators with variable compliance

The actuators that possess a variable compliance are able to regulate passively the physical compliance, having the capability of regulation of position, stiffness, wide of range of stiffness and very important energy storage. Such faculty brings out the benefit of the variable stiffness implementation comparing to the actuators with fixed passive compliance, it shows a similarity to the muscle-tendons apparatus, which assume a rigid configuration during contraction and compliant configuration during relaxation. This type of actuator can be categorized also in two main groups - in the first one, the compliance is placed in series between the actuator and the load and in the second one, it is set antagonistically as it is schematized in Figure 2.2 [15] [19] [20].

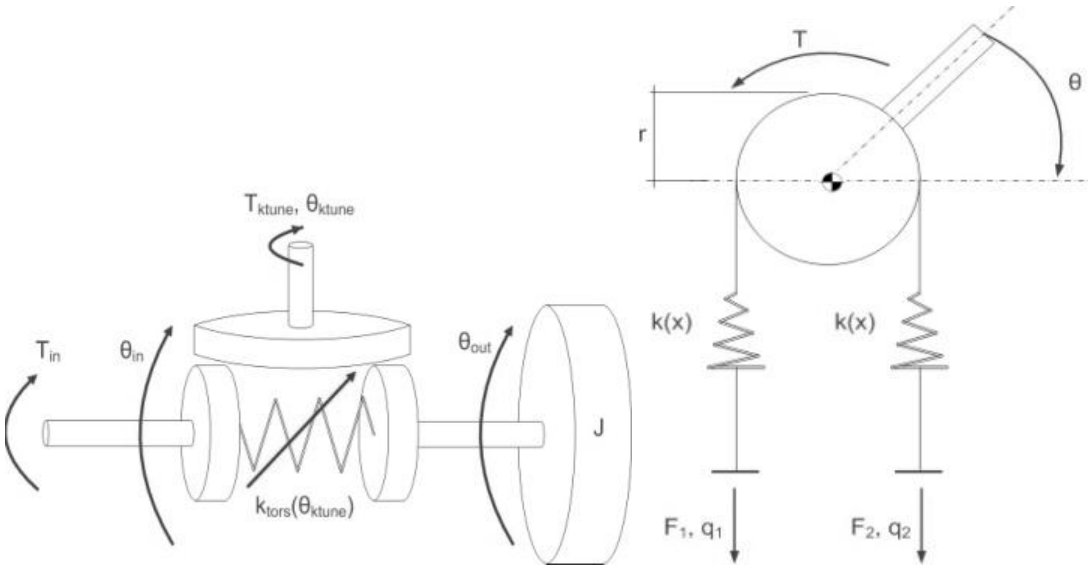

Figure 2.2 - Serial and antagonistic variable compliance actuation schemes respectively [20].

2.1.2.1 Series configuration

One of the main accomplishments of this type of variable stiffness actuator is the use of two actuators to set the equilibrium position of the joint, independently from the stiffness tuning. In the series configuration of actuators there are two ways to achieve the stiffness variation: one is through structure-controlled stiffness, which during operation can modulate the effective physical structure of a spring and achieve variations in stiffness and stored energy by adjusting the material properties (modulus, moment of inertia and/or effective beam length); the second way is through mechanically-controlled stiffness, which also adjusts the effective physical stiffness of the system, however, adjusts stiffness by varying the points where a compliant element is attached to the structure, as a result alters the pretension or preload of the spring [15] [19].

An example of the structure-controlled stiffness design is the *Jack Spring actuator*™ developed by Hollander, Sugar and their team [21]. In this new type of actuator, a helical spring is used as the compliant element and the lead of the Jack Spring changes under an applied axial load. The external force can act in both directions. Both compliance and equilibrium position adjustments of the Jack Spring™ mechanism is achieved by adding or subtracting the number of active coils, see Figure 2.3 [15].

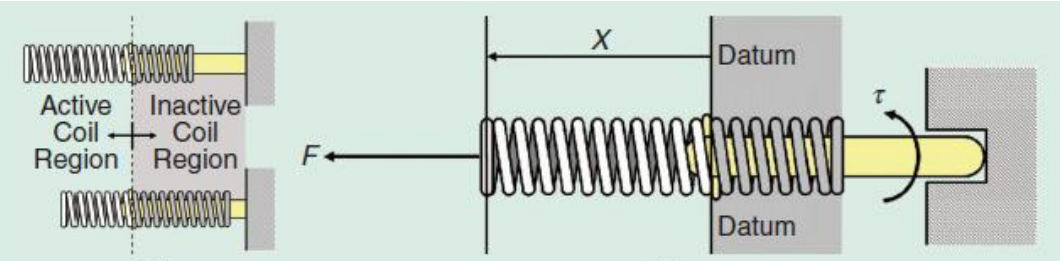

Figure 2.3 - Jack Spring™ Actuator's active and inactive regions [15].

The *Mechanically Adjustable Compliance and Controllable Equilibrium Position Actuator* (MACCEPA) developed by Van Ham et al. [18] is a application of the mechanically-controlled stiffness design, requiring only one compliant element (see Figure 2.4). The complete actuator behaves as a torsion spring where the spring characteristics and equilibrium position can be controlled independently during operation. The variation of the compliance is based on the variation of the length of the lever arms and uses only one passive element. Some advantages of MACCEPA actuator can be outlined: the actuator can be built with independently controllable

torque and stiffness, it has a significantly simple design and presents a linear angle-torque characteristic. On the other hand, has drawbacks regarding energy efficiency and the servomotors require some space in the structure [15] [17].

A new model of this actuator was proposed and the lever arm of the new setup is replaced by a profile disk. Therefore the torque-angle curve and consequently the stiffness-angle curve can be modified by choosing an appropriate shape of a profile disk. The advantages of the new setup are that the design is simple, can use linear springs and the control of equilibrium position and pretension are independent. The actuator shows both a large joint angle and stiffness range [18] [22].

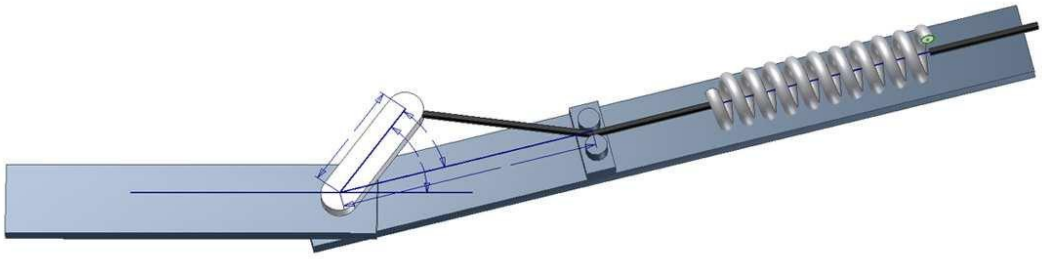

Figure 2.4 - MACCEPA actuator working principle [18].

2.1.2.2 Antagonistic configuration

In Antagonistic-controlled stiffness configuration two actuator units with non-adaptable compliance and non-linear force-displacement characteristics are coupled antagonistically, working against each other. By controlling both actuators and using nonlinear springs, the compliance and equilibrium position of this antagonistic setup can be changed. In order to obtain adaptable compliance, it is required the nonlinearity of the spring in the two actuators, while the resulting spring characteristic is linear. This design is biologically-inspired, following the concept of a joint actuated by two muscles arranged in an antagonistic manner [15].

The antagonistic design setups can be implemented using three different arrangements ‘Simple’, ’Cross coupled’ and ’Bidirectional’, see Figure 2.5. In an antagonistically-actuated joint are used two driving elements which by co-contraction regulates the stiffness of the joint and the angular displacement.

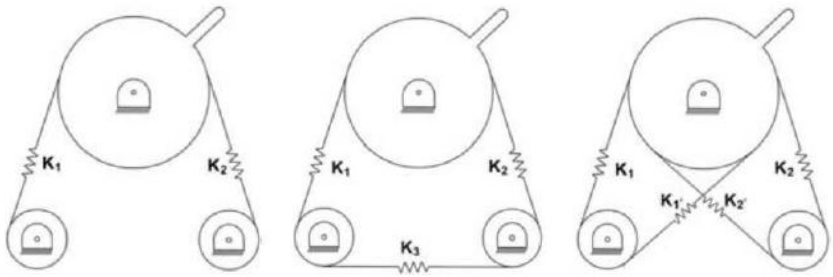

Figure 2.5 - The Simple, Cross-coupled and Bi-directional antagonist setups [19].

In the case of the 'Simple' antagonistic arrangement, the control of the compliance system can be performed by electric motors or more biologically inspired by pneumatic muscle actuators, which compliance is an inherent characteristic of the actuator.

The McKibben muscle [23] is the most well-known design of *pneumatic artificial muscles* (PAMs), that when pressurized contracts the muscle axially while expanding radially. The compressibility of air makes them inherently compliant, behaving in a spring-like fashion. However, one of the disadvantages is the substantial threshold of pressure, introduced by friction, which makes it difficult to control. The improvement of this mechanism is pleated PAM (PPAM) [24] which overcomes significantly the threshold of pressure. In this design, the angle and length of the lever arms can be altered to compensate for the strong non-linearity of the force-angle characteristic of the muscles in order to implement a more linear behavior of the joints torque and angular displacement [17].

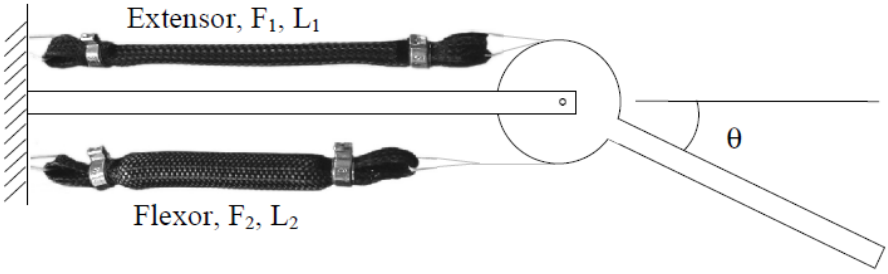

Figure 2.6 – Schematic of a rotational joint actuated by an antagonist pair of McKibbens [23].

However, in the 'Simple' antagonistic actuation approach using electrical actuation, differently from pneumatic actuation, the compliance is not an inherent property of the actuator and therefore requires additional compliant passive elements like springs between the actuators and the load. An example of this case of actuation is presented by *Migliore* [25], see Figure 2.7. Migliore is responsible for designing the "biological inspired joint stiffness control", which

describes the development and physical implementation of a servo-actuated robotic joint that uses antagonistic series-elastic actuation with a nonlinear spring mechanism. These mechanisms form a real-time mechanical feedback loop through independent control of both joint angle and joint stiffness [15] [17].

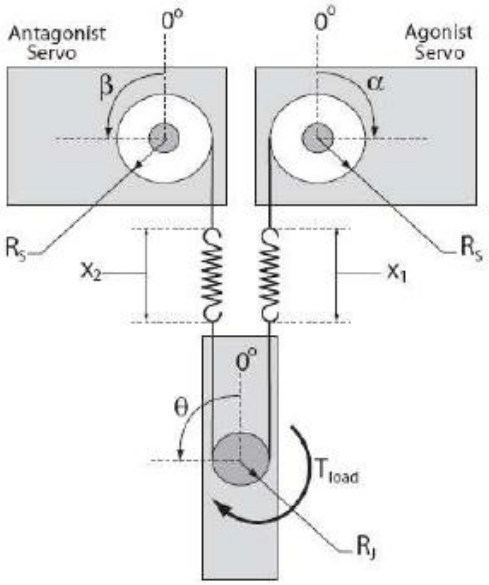

Figure 2.7 - Schematic of the Migliore's actuator [25]

A specific case of the cross-couple layout is the *Variable Stiffness Actuator* (VSA), presented in 2004 by Bicchi and Tonietti (Figure 2.8). A timing transmission belt (tensioned by springs) connects nonlinearly the main shaft to three antagonistic actuator pulleys, two are connected to position-controlled back drivable DC motor (pulleys 2 and 3 in Figure 2.8 – Variable Stiffness Actuator CAD views and schematic mechanism of one of the antagonistic pairs .Figure 2.8) and one connected to the link (pulley 1). The actuator antagonist motion of the drives changes the apparent angle between the spring axis and the belt and this permits the stiffness adjustment. Summarizing, it consists of elastic actuators in series which can modulate the position and stiffness of the system by acting on the springs and belt active length [17] [19] [24].

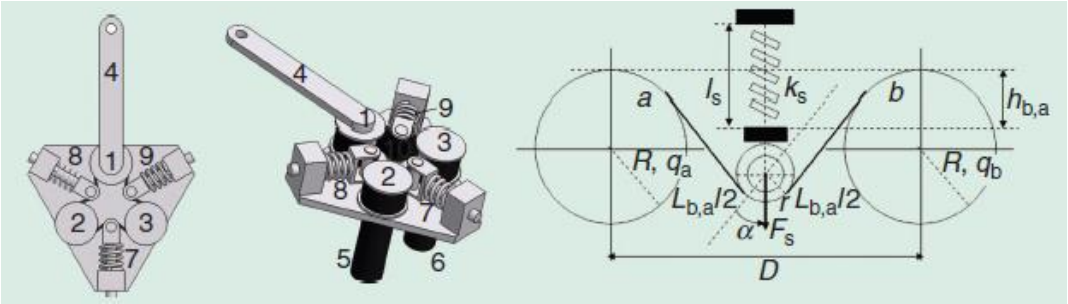

Figure 2.8 – Variable Stiffness Actuator CAD views and schematic mechanism of one of the antagonistic pairs [19].

Another important design based on the same principle of antagonistic design is the *Actuator with Mechanically Adjustable Series Compliance* (AMASC) developed by Hurst et al. The working principle is based still on the antagonistic setup of two nonlinear springs (Figure 2.9). The advantage is that just one actuator is used to control the equilibrium position and the compliance by changing the pretension of both non-linear springs. The AMASC reduction ratio of the pulleys varies proportionally with the spring deflection to obtain the quadratic relationship. The pulleys are also used to uncouple the control of compliance and equilibrium position [17] [26]. A linear version of this actuator is the VSSEA, (Variable Stiffness Series Elastic Actuator), developed by Thorson et al., in 2007 [27].

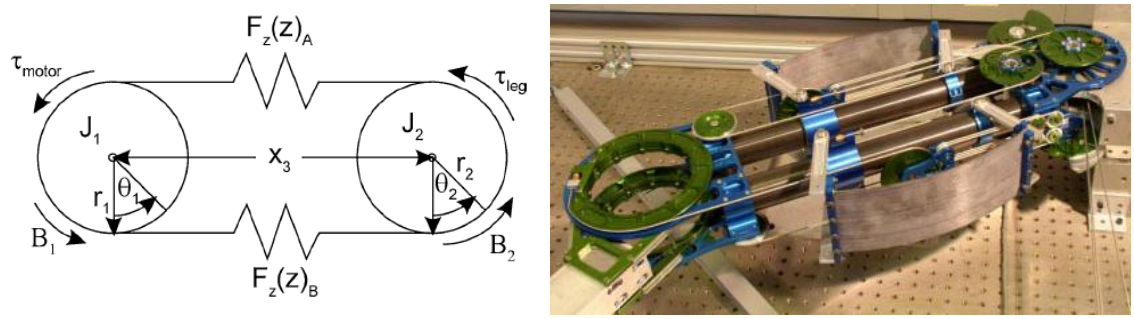

Figure 2.9 - Simplified schematic overview of the AMASC [19] [26].

2.2 Comparison of the passive compliant actuators

In the previous section, the configurations of the actuation systems were presented and simplified to their basic functionalities. From the beginning this devices can be classified in two

main groups, the fixed and the variable compliance actuation systems. Each of these two categories can be implemented following series or antagonistic designs.

Van Ham *et al.* in [15] did a complete overview and classification of adaptable passive compliant actuators classifying the various designs [18]. He provides an overview of some of the properties for the different groups of controllable stiffness actuators, Table 2.1.

Table 2.1 - An overview of some of the properties for the different compliant actuators [15].

	SEA	**Jack Spring**	**MACCEPA**	**Antagonistic**
Minimum spring number	1	1	1	2
Linear springs	Yes	Yes	Yes	No
Always total spring length	Yes	No	Yes	Yes
Preload/Pretension in equilibrium position	No	No	Yes	Yes
Completely stiff setting possible	No	Yes	No	No
Vary compliant setting possible	Yes	Yes	Yes	No
Infinite bandwidth for shock absorbance	Yes	Yes	Yes	Yes
Infinite bandwidth for chosen compliance	No	Yes	Yes	Yes
Independent control stiffness and equilibrium position	No	Yes	Yes	Yes/ No
Possibility to vary linearity of the stiffness curve	Yes	Yes	Yes	No

Within each group, there are distinctions, and the described designs might be optimized for a specific application. Besides the named functional parameters, other design criteria may be taken into account as the complexity of the design, cost, speed of the stiffness variation, maximum torque, and size of the complete system [15].

There are obvious advantages that passive compliant actuators with variable stiffness offer when compared with compliant actuators with a fixed passive stiffness. The decision between choosing adaptable or fixed compliance design is dependent on the range of compliance that is needed and the load allowed by the device. Therefore, depending on the application, adaptable compliant actuators are more favorable for larger stiffness range being able to regulate

the required stiffness and torque range and consequently the energy storage, on the other hand, if weight is important and a small range of required stiffness values are desired than a fixed compliant actuator is better [17] [18] .

In the first concept, the fixed compliance actuators are based on adjusting the equilibrium controlled stiffness through the position of springs. These actuators demonstrate an advantage when compared to variable stiffness due to the compact design and the simplicity to control presenting more stability to repetitive motions, however constantly requires energy to regulate its actuator position.

In addition, while in a series configuration is required one actuator and one compliant joint, the antagonistic designs extra work is needed to adjust the stiffness because they need at least two actuators and two compliant elements per degree of freedom. The main difference between the fixed stiffness design performance, SEA, which possesses a series configuration, and the antagonistic designs from AMASC is that the last can vary its stiffness while the SEA cannot. Also, the AMASC has mechanical energy storage, tunable compliance and low friction. [15] [19] [26] [28].

Inside the antagonistic actuator configurations in contrast to VSA design, AMASC equilibrium position and compliance can be set more or less independently, each by a dedicated servomotor that can be dimensioned appropriately.

Comparing the performances of the designs equipped with springs with PAM setup is not easy because the calculation of the energy consumption of compressed air is not obvious or trivial. Similarly to artificial muscles in which the spring and motor are combined in one element, the pressurized air is both responsible for the compliance and force generation. The maximum range of motion is limited by the maximum contraction and rest length of the muscle [17].

Opposing the mentioned two types of variable compliance actuators with a series configuration, the Jack Spring allows adaptable compliances and actively tunes the intrinsic stiffness of the spring and, on the other hand, the mechanically controlled stiffness, mentioned MACCEPA, is an actuator with independently controllable compliance and equilibrium position [15]. Also, the MACCEPA actuator has a second advantage in the fact that the construction is much more straightforward when compared to the other designs because the construction of quadratic springs is difficult and the MACCEPA actuator uses one simple linear spring. It has

both a large joint angle and stiffness range, although the actuator shows some drawbacks in the energy storing capabilities and the servomotors require some considerable space [17] [18].

Recently, advances in material technology have introduced new substances, making it possible to build structurally strong articulated mechanisms that are compact and lightweight. Examples of such materials that can be used to develop novel actuators are shapememory alloys, electrorheological fluids, electrostrictive and magnetostrictive materials, and electroactive polymers [15] .

2.3 Applications of passive compliant actuators

As it has been said, compliant actuators are implemented in walking and running robots inspired by nature. Therefore some compliant actuators were developed to specific locomotive machine applications.

For the most well-known, the series elastic actuator [10], in 1998, Pratt set the “Spring Flamingo”, a planar bipedal walking robot with fixed stiffness. Afterwards Sugar [29], developed in 2002 a novel selective compliant actuator that consists of a spring attached in series to a linear actuator driven by a DC servomotor and the equilibrium position of the spring is controlled to exert a desired force [10] [24] [29]. In 2009 [30] a new mechanical design was developed, a bipedal walking robot named M2V2 with 12 actuated DoF in the lower body: three at each hip, one at each knee, and two at each ankle [30]. Fixed compliance actuators have also a role in rehabilitation robotics as in ankle prosthetics [31], which used a SEA that employs parallel compliance (Figure 2.10).

Figure 2.10 – Examples of SEA application. Spring flamingo [32], M2V2 bipedal [30] and ankle-foot prosthesis [31] respectively.

On the other hand, antagonistically displayed series elastic actuators were implemented in a robotic leg mechanism as illustrated in Figure 2.11, which transmit the agonist/antagonist forces to the joint [19].

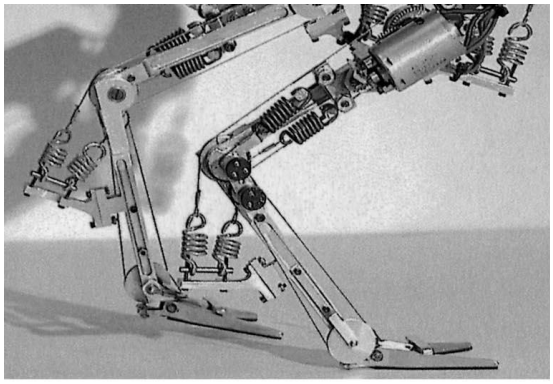

Figure 2.11 – Robot legs with antagonistic elastic actuators [12].

Other configurations that allow both joint stiffness control and spring pretension, such as the AMASC actuator [26]. Hurst and his team designed the biped robot with Mechanically Adjustable Series Compliance (BiMASC) which incorporates tuned mechanical leg springs, see Figure 2.12.a) [33].

Alternatively, Beyl and Vanderborght [34] [35] presented Lucy (Figure 2.12.b)), a two dimensional walking robot with two articulated legs, powered by pleated pneumatic artificial muscle (PPAM) to actuate 6 DoF (ankle, knee and hip joint) [34] [35].

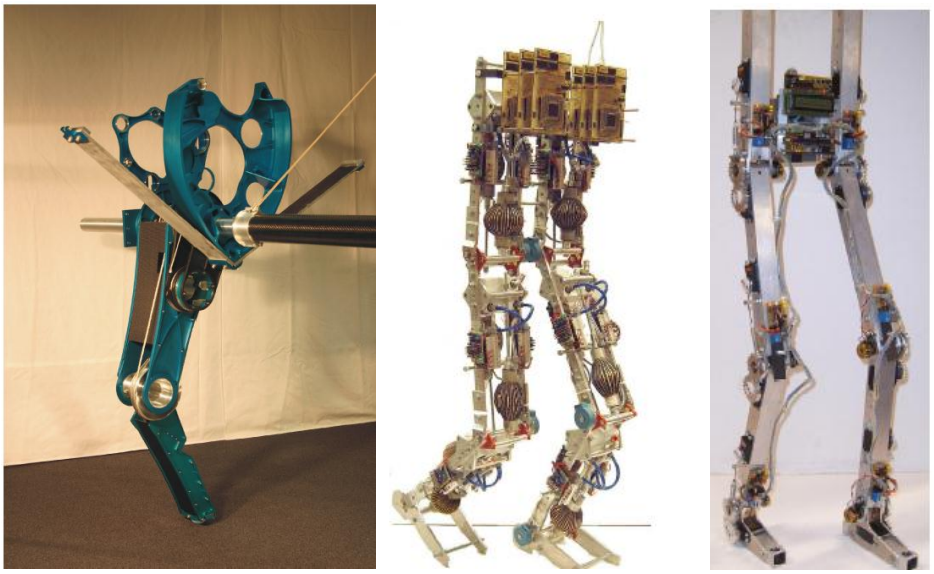

a **b** **c**

Figure 2.12 – a)One of the BiMASC's legs, partially assembled [33], b) Bipedal walking robot Lucy actuated by PPAM's [34], c) Bipedal walking robot Veronica actuated by MACCEPA's [34]

Biped Veronica Actuated based on MACCEPA's actuator (Variable joint Elasticity RObot with a Neuro-Inspired Control Approach) illustrated in Figure 2.12.c), similar to Lucy, however uses a novel control approach, can be adapted at will by systematically setting the equilibrium positions and compliance values of the different joints, resulting in a variety of semi-passive gait patterns [18] [34].

After the analysis of the different designs of compliant actuator systems, for the project of Bioloid, weight has an important part and the stiffness values required to accomplish the load support by the legs are small, the fixed compliant actuator type proves to be the most adequate to be applied for this application. Also, presents a major advantage in stability matters (in repetitive motions as the locomotion cycle) due to its compact design and simple control.

3 Quadruped leg configuration

The aim of this section is to study the various concepts that are taken into account to enable the compliance factor applicable in the robot in terms of the configuration of the leg to a successful retraction. Thus, basic consideration for a leg design can be outlined as follows: the leg should generate an approximately straight-line trajectory for the foot with respect to the body and the leg should have an easy mechanical configuration, towards building a robust and feasible robot [1] [36] [37] [38] [39] [40].

3.1 Legged Robots

A good design is important when it comes to any robot. In the locomotion study and design most legged robots mimic animals in structure. Although many challenges remain, some concepts from biologically inspire robotics aiming to eventually benefit the design of autonomous robots with some of the desirable properties of biological behavior, such as adaptability, robustness, versatility, and agility. A good design would mean: simple control, reduced dynamic effects, high stability, power equilibrium, simplified movement and low cost.

Over the time, taking the inspiration from biology based on scientific observation on legged animals, legged robots in combination with innovative engineering has been witnessing a significant increase in the interest and efficiency, resulting in several artificial walking machines

[12] [39] [41] [42]. The rising interest in legged systems is to expand the understanding of human and animal locomotion, perhaps in cases of great mobility and agility [2] [43] [44]. Basically, taking into account the features of the animal locomotion, there is a need to design and develop a highly flexible and sophisticated walking machine to mimic the muscular behavior [42] [45].

Although the locomotion in legged animals is very simple, researcher's previous efforts resulted in a number of legged robots with wide variation in shape, size and complexity [42].

In the development of legged machines it must be taken into account several points, which influence the technical features of these systems. As the most important of these variable parameters, it can be listed:

- mechanical structure - determines the walking machine posture, energy efficiency, range of walking speed and types of gaits which can be later implemented
- leg configuration - choice of number of legs, their kinematics structure, joint design solution
- actuating and drive mechanisms - choice of motors type, evaluation of their power, design of motor placement and evaluation of methods of motion transmission from motors to the legs joints to perform an autonomous navigation.
- power consumption in relation to the machines weight, payload, motion conditions - soft, hard terrain, inclined terrain, etc.
- method of walk - speed of motion, balance, number of legs supporting the body during walk, etc. [2] [45] [46].

3.2 Robotic leg mechanism

As mentioned different disciplines (engineering, biology, zoology and computer science) have been involved to discover the complexity of natural locomotion behavior and is a growing field in biomechanics. The promising approach of biologically inspiration aims to use the observed natural principles of locomotion for the efficient design and control of walking machines [47].

In small mammalian quadrupeds, two types of so called effectors are distinguished, muscles and glands. Relevant for the actuation of the locomotion system are the skeletal muscles together with the tendons. In fact, small mammals present similarities to a pantograph mechanism, which is more or less rectangular (see Figure 3.1), during rotation around the legs joints at the trunk. In the stance phase the generation of displacement of the animal is conducted by a spring-mass system. The springs are muscles, the more stiff show a higher compliance factor that offers the possibility to elastically store more energy. The study of pantograph mechanism and implementation will be further addressed [47] [48].

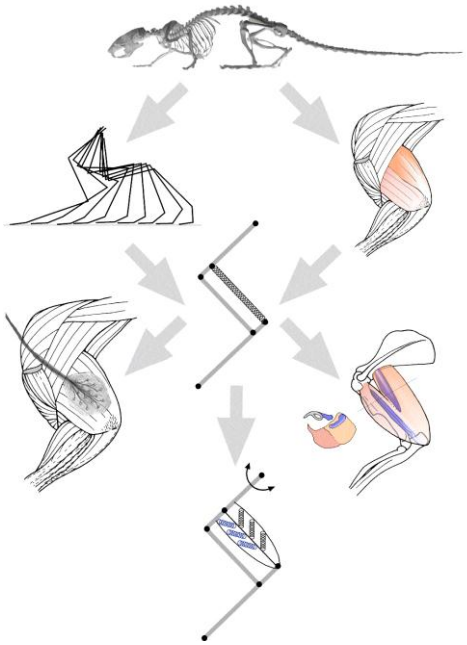

Figure 3.1 - Concept of the "pantograph leg" of small mammals [48].

There are several characteristics and principles that can be extracted from mammalian locomotion, in order to implement a stable and adaptive walking in the new leg:

- The limbs of mammals are almost tri-segmented shaped and present the same configuration in terms of functionality, both in fore-limb and hind-limb, therefore the construction may be the same (see Figure 3.2).
- The progression is mainly due to the displacement of the proximal segment (scapula or femur) being the leg drive.
- Two segments (first and third - femur/foot) operate almost parallel during retraction of the limb, as in a pantograph mechanism.

- High limb compliance is a general principle for small mammals, and this helps the self-stabilization of the limb, i.e., the stable locomotion of the animal, in presence of external disturbance without the necessity of a sensory feedback [12] [48].

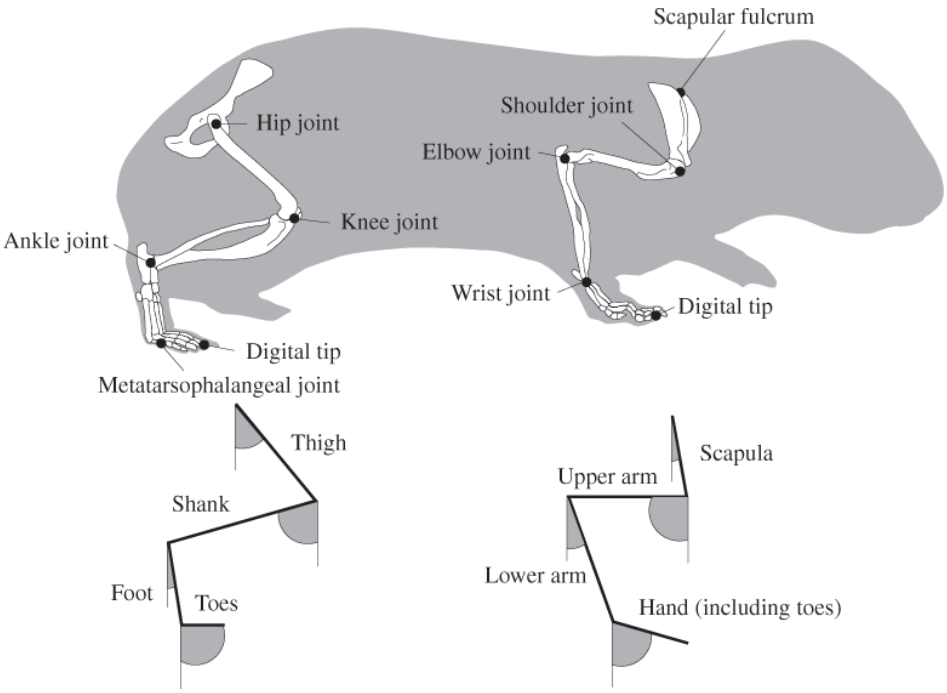

Figure 3.2 - The tri-segmented limb abstraction for small mammals. The limbs are segmented in three parts – Fore-limbs/Hind-limbs : scapula/femur, humerus/shank and lower arm/foot [12].

Considering the number of segments in the use of a two-segment leg, compression directly translates into joint flexions which in turn results in a higher joint torque and, consequently in an increased leg force (Figure 3.3).

Three-segmented limb in a z-configuration are typical presented in front and hind limbs of mammals. The additional segment adds a degree of freedom in which the internal joint angles and the three segment lengths work together in the foundation of this configuration.

The additional degree of freedom in tri-segmented limbs imposes the risk of structural instability for z-shaped legs in case of a very dynamic motion, where the compression may result in different situations (e.g. bifurcation). However the triple linkage of the leg shows a higher effective energetic and mechanical advantage.

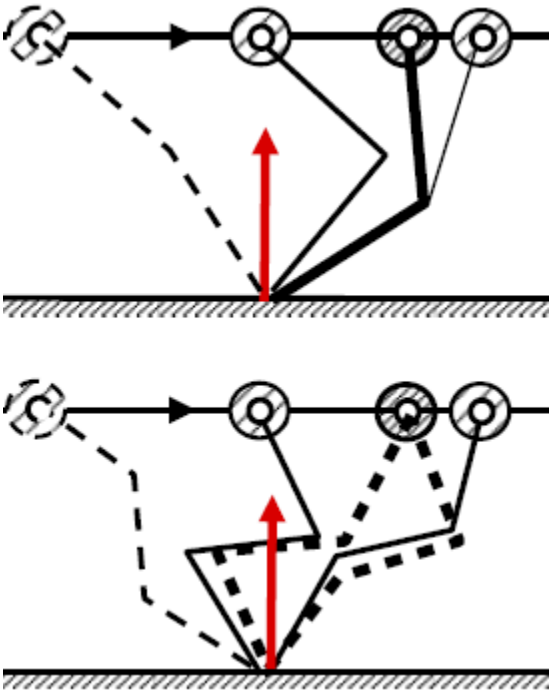

Figure 3.3 – Schematic description of a bi-segmented system configuration with a single joint and a tri-segmented with a par of joints respectively [49].

The highly mentioned ‘‘pantographic behavior’’, more specifically the synchronous movement of the two joints of the tri-segmented leg, insures that this instability does not occur, i.e. the first and third segment operate in matched motion, where the inner angles are always equal [19] [49] [50] [51] [52].

There are constraints on the possible combinations of joint angles and segment lengths that are relevant for legs physics. The relative length of limb segments is special relevant in the leg design. Another advantage for small animals with three-linkage limbs is the equally long segmentation which indeed contributes to a lesser degree to progression. The benefits of this configuration are a large working range and good acceleration properties with less energy cost [50].

3.2.1 Types of leg structures

During walking, a four-legged walking robot places its weight on three and four supporting legs alternately. Thus, it implies that in each locomotion cycle, there are instances

when any leg has to carry a load that can be as high as four times the leg's own weight. In this section is presented a variety of leg geometries that can provide the motion required by a quadruped walker. Some of these mechanisms are:

- **Straight Line Mechanism** realizes body-propelling motion by one degree of freedom. With reduced degrees of freedom the control system becomes simpler. However, straight line linkage mechanisms have limitations like complex arrangement of links and restricted workspace. Also, adaptability to the terrain also becomes poor with such systems.
- **Articulated legs** have the advantage of a larger workspace. The arrangement of two coincident hip joints has the benefit of placing two of the leg actuators on so that their mass is not carried by the leg during foot transfer. Also, the perpendicular disposition of joint axes at the hip provides a larger leg bandwidth workspace and simplifies the leg kinematics. There are two variations of this leg: insect-type and mammal-type. In the insect-type leg, the knee joint is located laterally or at a position higher than the hip (Figure 3.4a), whereas, in mammal-type legs, the knee joint is placed under the hip (Figure 3.4b). Due to geometric work loss, articulated leg designs are often responsible for poor energy efficiency of the robot.

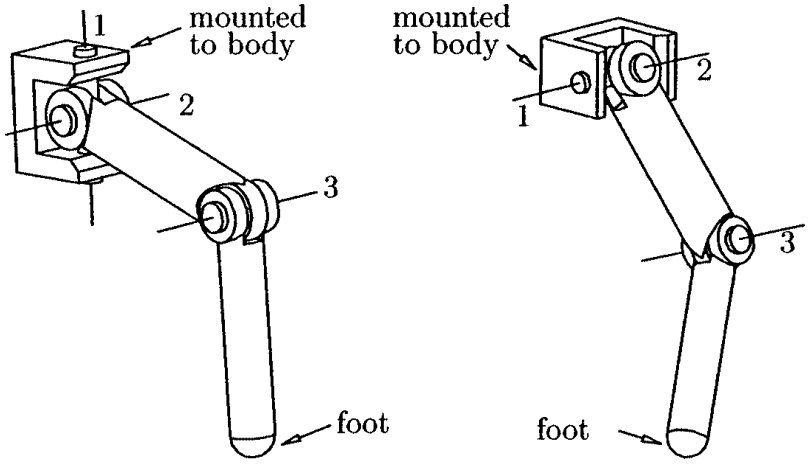

Figure 3.4 - a) insect-type and b) mammal-type articulated legs respectively [42].

- **Gravitationally Decoupled** method that dissociates the leg actuators that propel the body from the actuators supporting it during propulsion. Such mechanism allows elimination of negative power by ensuring that the load-bearing actuators do not move

and the actuators which move do not bear load. In the past, a number of leg mechanisms were used to perform such gravitationally decoupled actuation:

- *Orthogonal* - The legs are displayed in an orthogonal RPP (rotational-prismatic-prismatic) mechanism that decoupled horizontal and vertical motions. As shown in Figure 3.5, the configuration consists of a rotation link, an offset extension link, and a support link. There are three degrees of freedom per leg, with two rotational joints and one prismatic which held the foot.

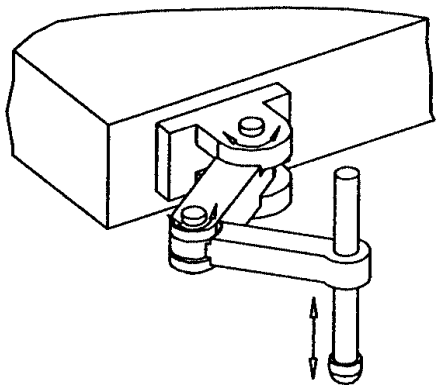

Figure 3.5 - Orthogonal configuration RPP [42].

- *Two-Dimensional Pantograph* - provides straight line foot motion along the forward and vertical directions. Foot motion in the lateral direction (if any) is due to rotation of the leg about an axis parallel to longitudinal body axis (Figure 3.6.a). In other case, the leg is designed for motion in the vertical plane which can rotate about the vertical hip axis (Figure 3.6.b).

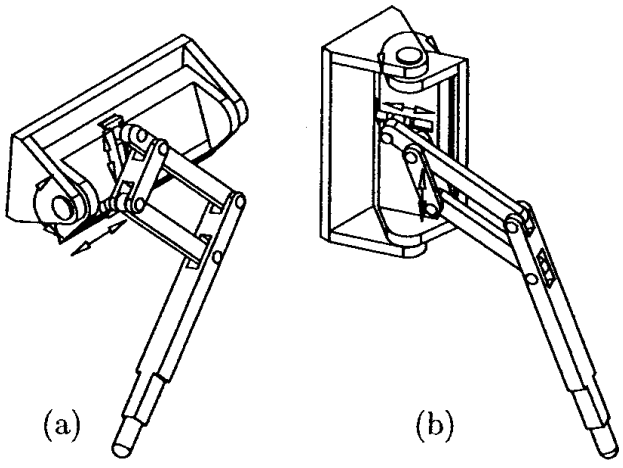

Figure 3.6 - Two-dimensional pantograph mechanism legs [42].

- *Three-Dimensional Pantograph* - In the three-dimensional pantograph, all the three motions are linear (Figure 3.7). The most important advantage of the pantograph mechanism is that geometric work loss can be completely eliminated. However such benefit can only be achieved if there are none tangential ground reaction forces. An important feature of three-dimensional pantographs is the particularity complexity of the mechanical design.

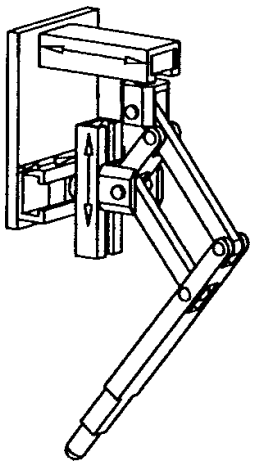

Figure 3.7 - Three-dimensional pantograph leg [42].

3.3 Cheetah robot

Over the years several legged robots applications were developed using the pantographic configuration. Due to the rising improvements and the successful simulations accomplished, the Cheetah pantographic mechanism, proved to be an interesting object of study, development and ultimatly an application to follow.

Oncilla robot, inherited "Cheetah", features a lightweight mammal-like robot three-segmented pantographic legs (see Figure 3.8) of a domestic cat (*Felis catus*). The first version of Cheetah was built by Simon Rutishauser [11] applying several principals in the design of a bioinspired quadruped robot. Since then, the robot has been upgraded several times, although the main features remain unchanged. For the work developed in this dissertation, some of the Cheetah's main design concepts and work principles were introduce in the new mechanism.

3.3.1 Three-segment leg

In Figure 3.8 is represented one of the most modern Cheetah robot design. As it shows, in both limbs a distinct three segmented construction is featured (plus one toe segment). For the hind limb is presented a hip joint and thigh (l_3), a knee joint and shank (l_2, l_4), and an ankle joint and foot (l_1). The joint in each pair describes the proximal assembling point of the corresponding leg segment. The extra joint is connecting the toes as the fourth, most distal hind limb joint. For the robot's front limb the same relative segmentation is done [12] [14] [53].

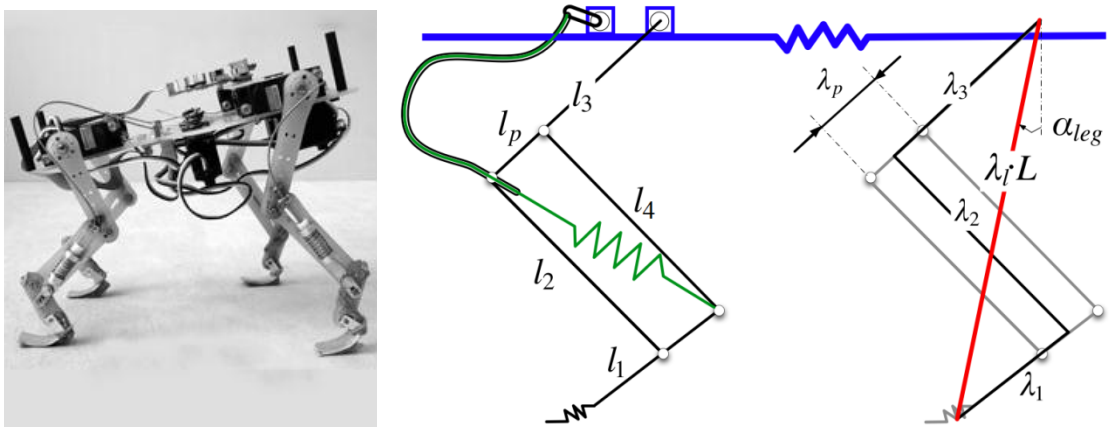

Figure 3.8 - Cheetah robot prototype and side view of the architecture schematics respectively [11].

In this robot is implemented a pantograph mechanism, constantly ensuring parallelism between two leg segments. More precisely, the pantograph holds the connection between proximal and distal limb segment, maintaining the first and third leg segment parallel during motion (l_1 and l_3, e.g. thigh and foot). This mechanism assembly resembles animal leg segment behavior for most of a step cycle. Here, only one DoF influences the leg length and there is no need to deepen the study of the leg configuration stability [50] [53]. Also, the leg relative dimensions are designed based on biological data from small mammal, distance and ratio between the leg segments of the pantograph mechanism is compromised to guarantee mechanical strength and energy efficiency [14] [50] [54].

3.3.2 Pantographic model actuation with a passive spring mechanism

In Cheetah's, the technical locomotion system is characterized by an actuation principle consisting in the use of an actuator with a pantograph mechanism as a method of linear actuation with amplification [39] [47].

Each foot is actuated in all three axes with servomotors. There are a total of twelve motors involved in the locomotion, three motors for each leg controlling the three axes. Since the three axes are controlled individually, motion in the X, Y and Z axes are decoupled, which increases the simplicity of control [39].

In locomotion for the model above described, each leg features tri-segmented pantograph together with two actuated joints per leg (in the hip and in the knee) and also a passive compliant mechanism at the knee joint level. All actuators are located on the main part of the robot body (the trunk) and the actuation of the knee is made through Bowden cables [12] [14]. The proximal actuator placed at the hip joint (hind limb), is responsible for leg protraction and retraction. The second actuator is flexing the two mid-joints via the mentioned cable mechanism (internal force), also acting as a de-coupling mechanism for external forces, applying and flexing the pantograph joints [53].

The robot's pantographic legs are equipped with a passive compliant mechanism by adding a compression spring on the diagonal of the pantograph mechanism (Figure 3.8) [53]. This passive compliant system, at the knee-joint, works throughout a spring in parallel with the retraction mechanism with the goal of enabling different dynamic gaits [50]. The orientation and the type of springs used classifies the robot's leg as a passively extending, gravity loaded, compliant leg [53]. In other words, in the passive compliant knee joints is possible to both extend and retract the leg by acting as a counterforce during retraction and by during extension of the leg apply no actuation at all, supporting the springs expansion [13] [14].

In Cheetah quadruped robot, the motor is pulling a Bowden cable that tends to reduce the diagonal of the parallelogram of the tibia segment, and then contract the leg. In Figure 3.9 shows the operation modes of the compliant mechanism:

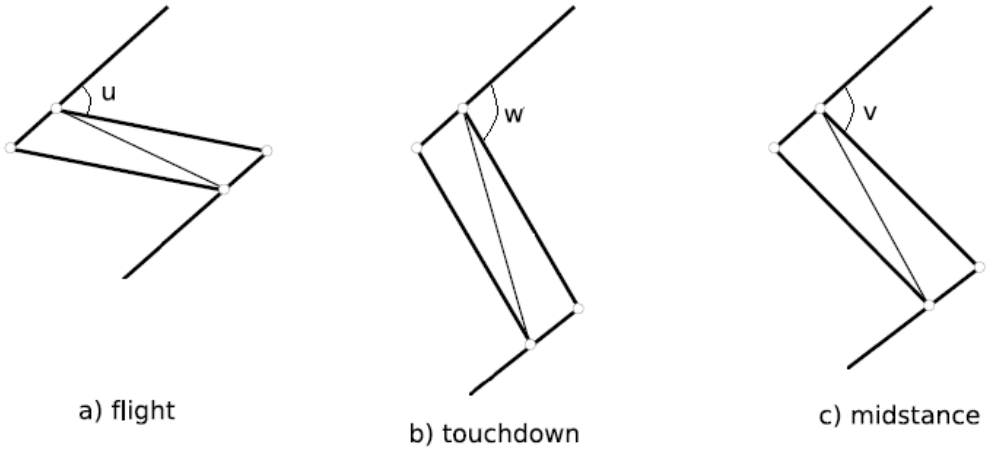

Figure 3.9 - Diagram of the performance of the compliant mechanism of the pantographic leg (u<v<w) [50].

The compliance of the leg is within the knee mechanism as a self-stabilization of the locomotion. As shown in Figure 3.9, it can be defined three operation modes at the knee joint:

1. Actuated position joint: The servomotor is on, reducing the diagonal of the parallelogram of the tibia segment, and then contracting actively the leg (Figure 3.9.a). The motor at the knee joint only actuates to retract the leg during flight phase.

2. Resting position joint: If there is no action of the servomotor, and no action on the distal segment, then the spring extends the leg at its maximum (Figure 3.9.b). The spring extends the leg before touchdown and it is ready to become gravity loaded.

3. Joint under external forces: In the presence of external interaction (if the robot stands on the ground), then the spring is actively compressed, and the motor is disconnected from the system. The equilibrium is obtained by the spring, counter-acting the gravity force from the weight of the robot to operate as compliance in major forces from the locomotion velocity (Figure 3.9.c) [12].

At the last part of the stance phase, before liftoff, the spring restitutes some of its energy, thus contributing to the forward motion and the locomotion cycle restarts [50]. The compliance adopted in the spring-mass model of Cheetah robot shows a major benefit to improve robot walking.

For the Bioloid quadruped leg design some considerations may be extracted. Some principles of small mammals like the pantographic model may be taken into account in the construction, in an effort to provide stability to the leg configuration. Cheetah design shows to be

of great interest for this work. The three-segmented pantographic legs are interesting concepts to be integrated in the modeling design. Also following the foundation of Cheetah quadruped, the operation modes towards the compliant mechanism actuation at the leg, shows a major contribute for the simulation control during locomotion.

4 Leg modeling

This chapter exploits the modeling and configuration of the proposed legged robot, explaining the main principles of the applied physics in order to accomplish a stable and reliable structure. In more detail the fundamental equations of the kinematic study of the three-segmented leg stability is assessed and also the information regarding the generation of the movement, limits of motion and the main foundation of the evolution of the retraction. Also, the spring and damping coupled to the mechanism is analyzed based on the study of the joint angle variation and external forces applied during locomotion.

4.1 Novel model of the Leg

As mentioned before the goal of this master dissertation is to improve the leg design of the Bioloid robot and adapt some of its features in the leg of a quadruped robot. From the previous section insights it is now possible to determine that the project developed features an innovated mammal-like robot three-segmented, pantographic leg design with passive compliant joints. Each leg has three degrees of freedom: hip joint (pitch and roll) and knee joint (pitch) that can be actuated. The leg of the robot is a pantograph leg i.e. the first (foot, l_1) and the third leg segment (thigh, l_3) are forced to be parallel, resembling the animal leg behavior for most of a step cycle [53] [55] [56]. Also, the hip active joint main actuation is on the protraction and retraction of the

leg, providing to the robot the intended locomotion and displacement, while the knee has the function of extend and contract the leg having the main role in the retraction and extension and therefore in the impact neutralization [11].

Thus, taking into account these considerations, it was possible to settle the model for the new Bioloid leg. Figure 4.1 shows the new leg segmentation employed where the red line represents the associated virtual telescopic leg. As it can be clearly seen, the leg segments l_1 and l_3 are always parallel and the inner angles of the pantograph are always equivalent.

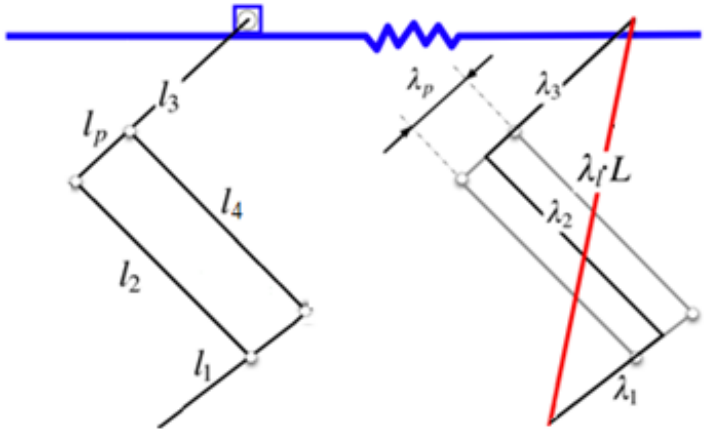

Figure 4.1 - Pantographic three-segmentation for the Bioloid leg.

The pantographic mechanism is responsible to preserve the stability. At [57] it was considered an energetically advantageous approach in which for smaller mammals was introduced the equal segment lengths for the limb measurements. Analytically the normalized lengths of the limb are:

$$\lambda_1 = \lambda_2 = \lambda_3 = \frac{1}{3}. \tag{4.1}$$

Spröwitz [58] shows that the resulting leg stiffness of the virtual leg mainly depends on the choice of λ_2, λ_p and the virtual leg spring stiffness k_{leg}, but not on the segments λ_1 and λ_3. The equalization of the segments λ_1 and λ_3 sizes was done according to:

$$\lambda_1 = \lambda_3 = \frac{1-\lambda_2}{2} \tag{4.2}$$

There are clearly stable solutions for λ_2 and λ_p more desirable for a wider range of stable angles of attack for a particular leg stiffness according to the velocity intended for the quadruped robot. Küchler [57] performs a study for a stable running in the Cheetah robot, in an energy conservative system, where the λ_2 values for different situations are considered taking into account that for the pantograph leg the following geometrical constraint needs to be fulfilled:

$$\lambda_p \leq \lambda_1 = \frac{1-\lambda_2}{2} \tag{4.3}$$

From the relative dimensions of the three segments, the absolute segment lengths are able to be deduced. In Figure 4.1 it is possible to observe the relation between the segment relative and absolute lengths. The subtraction of the relative distance between shank segments l_2 and l_4, called $\frac{\lambda_p}{2}$ in the terms for λ_1 and λ_3, is due to the fact that the studies on relative segment lengths do not consider pantographic legs specifically, but rather work with only the middle segment, simplifying the kinematic study. This subtraction is a mean between linkages, considering leg segment l_2 as the mid segment and neglecting segment l_4, or the other way around [50]. To obtain the final three links values, the relation between the segment lengths relative to the maximum leg length is defined as:

$$\lambda_1 = \frac{l_1}{l_1+l_2+l_3} - \frac{\lambda_p}{2} \tag{4.4}$$

$$\lambda_2 = \frac{l_2}{l_1+l_2+l_3} \tag{4.5}$$

$$\lambda_3 = \frac{l_3}{l_1+l_2+l_3} - \frac{\lambda_p}{2} \tag{4.6}$$

$$\lambda_p = \frac{l_p}{l_1+l_2+l_3} \tag{4.7}$$

Since the starting point was the original Bioloid robot the thigh segment length can be extracted (see Figure 4.2), i.e. the measurement of the length between the axis at the hip joint and the axis at the knee joint corresponding to the l_3 segment is known in advance from the previous

model. As it will be further proved, through the knowledge of this value and the maximum length intended for the leg all the remaining linkage measurements as well as the extension range may be defined.

$$l_3 = 0{,}083m$$

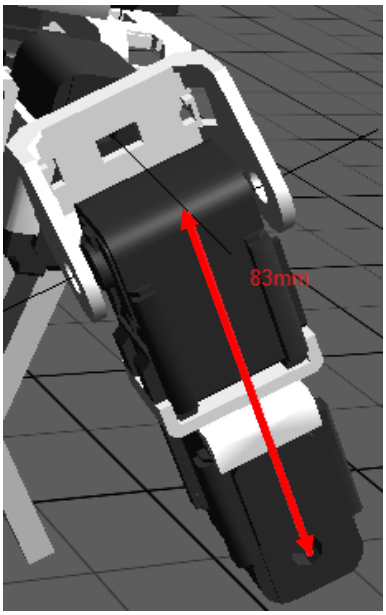

Figure 4.2 - Thigh segment of Bioloid leg model in Webots™.

The use of compliance in legged systems has the advantage that the leg can temporarily store and release mechanical energy during the stance phase. To consider the needed compliance to apply, the force applied in a robotic leg must be firstly calculated. Such study requires the knowledge of several parameters: the segmentation of the leg (length and orientation); the quadruped weight and the load applied in a single leg; and finally the spring-damp system wanted.

4.1.1 Kinematic analysis for the leg model

The pantograph leg can be reduced to a virtual leg (red line in Figure 4.1 and point A to B, in Figure 4.3). The virtual leg is a telescopic leg with equivalent properties to the pantograph leg in terms of the leg force. Several studies referring to the pantographic leg are developed through the reduction to the virtual leg.

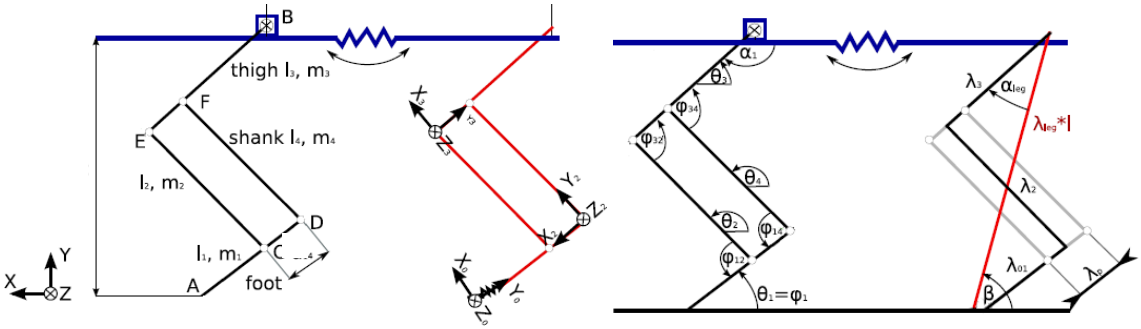

Figure 4.3 - Hardware sketch of the angles and the different points and segment lengths for the side view of the leg. The red line is the virtual single-segmented leg [50] [57].

Thus, the definition of the leg length can be expressed relatively to a complete extension of the limb. For this model the total length of the legs was settled:

$$L_T = l_1 + l_2 + l_3 = 0{,}21\ m \tag{4.8}$$

Using the local coordinate system (Figure 4.3) the relative leg length $l_\lambda = \frac{|AB|}{l_1+l_2+l_3-l_p}$ can be expressed in function of the angles $\varphi = \varphi_{14} = \varphi_{34}$ and the relative leg segment lengths:

$$\mathrm{L}\lambda_l = \lambda_1 + \lambda_2 + \lambda_3 = \begin{pmatrix}0\\1\end{pmatrix}\lambda_1 + \begin{pmatrix}\sin\varphi\\-\cos\varphi\end{pmatrix}\lambda_2 + \begin{pmatrix}0\\1\end{pmatrix}\lambda_3 \quad [m] \tag{4.9}$$

the modulus of the leg vector gives the relative leg length, function of the angle φ:

$$l_\lambda = |\mathrm{L}\lambda_l| = \sqrt{(\lambda_2 \sin\varphi)^2 + (\lambda_1 - \lambda_2\cos\varphi + \lambda_3)^2} \tag{4.10}$$

whereas the inverse equation $\varphi\ (l_\lambda)$, for the instantaneous joint angle is:

$$\cos\varphi = \frac{\lambda_1^2+\lambda_2^2+\lambda_3^2+2\lambda_1\lambda_3-l_\lambda^2}{2\lambda_2(\lambda_1+\lambda_3)} \tag{4.11}$$

while α_{leg} (in Figure 4.3) represented by the angle between the virtual leg A to B and the thigh segment l_3 amounts to:

$$\sin\alpha_{leg} = \frac{\mathrm{L}\lambda_l\begin{pmatrix}1\\0\end{pmatrix}}{l_\lambda} = \frac{\lambda_2\sin\varphi}{l_\lambda} \tag{4.12}$$

4.1.2 Virtual Leg Step Cycle

A simple model for running with compliant legs brings the spring-mass model, also known as spring-loaded inverted pendulum (SLIP), is illustrated in Figure 4.4. The running stability for the SLIP model is examined by Seyfarth in [59]. The improvement over the telescopic leg is achieved due to the non-linear relation between leg force and leg length, resulted from the leg segmentation.

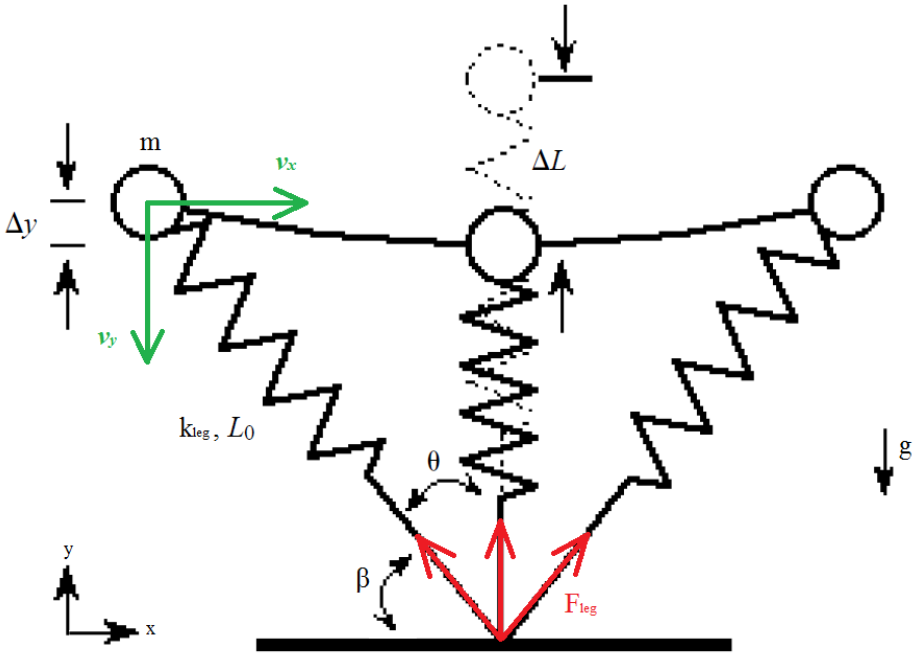

Figure 4.4 – Variation on the virtual SLIP leg model during one step [12] [56].

The SLIP model is kept very simple: The body is represented by a point mass m, the axial leg operation during the stance phase is approximated by a linear spring of constant stiffness k_{leg} and length L_0 when fully extended. This virtual leg is massless and it has no moment of inertia. Effects of friction or other non-conservative forces are neglected therefore the system is energy conservative. The leg touches the ground with a constant angle of attack β_0. During the stance phase the leg angle changes naturally with the motion. After the flight phase the angle of attack is reset to β_0 and the cycle restarts.

Trotting and hopping are often modeled as simple spring-mass systems bouncing along the ground. The Figure 4.4 shows the models movement of the mass during the stance phase (moving from left to right). The leg spring has an initial length (L_0) at the beginning of the stance phase,

and its maximal compression is represented by ΔL. The dashed spring-mass model illustrates the length of the uncompressed leg spring. As a result, the difference between the length of the dashed leg spring and the maximally compressed leg spring represents the maximum compression ($\Delta L = L_0 - L$). Moreover, the downward vertical displacement of the mass during the stance phase is represented by Δy, which is expected to be considerably smaller than ΔL. Half of the angle swept by the leg spring during the ground contact time is denoted by $\theta = \frac{\pi}{2} - \beta_0$, which is equivalent to the difference between the vertical axis and the initial angle of attack [56].

Every stance phase begins with the touchdown of the leg. In the SLIP model, at the beginning of stance phase, the leg touches the ground with the angle of attack β_0 (Figure 4.4). During this part of the step cycle the foot is fixed on the ground. The effects of friction, damping or slipping by the contact are not taken into account. Thus, the only active force besides gravity is the leg force F_{leg}. The equation of motion for the system is given by:

$$\begin{bmatrix} F_x \\ F_y \end{bmatrix} = \begin{pmatrix} m\ddot{x} \\ m\ddot{y} \end{pmatrix} = \begin{pmatrix} -F_{leg}.\cos\beta \\ F_{leg}.\sin\beta - mg \end{pmatrix} \quad [N] \tag{4.13}$$

With

$$F_{leg} = k_{leg}.(L_0 - L) \quad [N] \tag{4.14}$$

The peak of force in the leg spring occurs at the middle of the stance phase when the leg spring is oriented vertically, and thus corresponded to the peak vertical ground reaction force. It is important to notice that this method of calculating k_{leg} gives a measurement of the total stiffness during the stance phase and not of the stiffness of an individual limb [56] [57].

The peak displacement of the leg spring (ΔL) can be related to the peak displacement of the center of mass (Δy) through the length of the leg spring at the instant that it hit the ground (L_0) and half of the angle swept by the leg spring while it is in contact with the ground (θ):

$$\Delta L = \Delta y + L_0(1 - \cos(\theta)) \quad [m] \tag{4.15}$$

During the flight phase the leg force has no effect on the system dynamics ($F_{leg} = 0$). Therefore the equations of motion are those of a ballistic flight of a point mass:

$$\begin{pmatrix} m\ddot{x} \\ m\ddot{y} \end{pmatrix} = \begin{pmatrix} 0 \\ mg \end{pmatrix} \tag{4.16}$$

4.1.2.1 Reference stiffness and limitations in the retraction

Fallowing the procedure at [50] a leg angle at touchdown of $\varphi_{touchdown} = 130°$ is assumed for small quadrupeds. Considering the previous analysis, the relative leg length at touchdown may be determined by:

$$l_{\lambda,touchdown} = \sqrt{(\lambda_2 \sin\varphi)^2 + (\lambda_1 - \lambda_2 \cos\varphi + \lambda_3)^2} = 0{,}9172$$

$$\alpha_{leg,touchdown} = 16\,^{o}$$

As demonstrated in the last section, for a given three segment leg the leg force can be determined for any given variation in the virtual leg length ΔL. The work presented at [56] illustrates that the compression of the spring (ΔL) is about 16% of leg length in dogs during trot speed locomotion, consequently, a reference compression is defined ($\Delta L_{16\%} = 0.16 L_0$). Based on this reference compression and the corresponding leg force $F_{leg,16\%}$ of the pantographic leg model, the reference stiffness can be defined as:

$$k_{leg,16\%} = \frac{F_{leg,16\%}}{\Delta L_{16\%}} \quad \left[\frac{N}{m}\right] \tag{4.17}$$

with $\Delta\varphi = \varphi - \varphi_0$. To calculate the angle for the stiffness 16% retraction at middle joint:

$$\cos\varphi_{16\%} = \frac{\lambda_1^2+\lambda_2^2+\lambda_3^2+2\lambda_1\lambda_3-(l_{\lambda_{16\%}})^2}{2\lambda_2(\lambda_1+\lambda_3)} \tag{4.18}$$

With the equivalent angles $\varphi_{16\%} = 95°$ and $\alpha_{leg,16\%} = 26\,^{o}$

It must be noticed that when the desired 16% variation of the leg retraction occur, the step must be at mid-stance, more precisely, when the virtual leg is vertically aligned, therefore the angle of attack β is of 90°. Considering the previous equation (at chapter 4.1.2, equation 4.13), it is possible to achieve the force and spring constant values of the constrained leg.

Also, knowing that low velocities are in play for this case of walking locomotion, the swing angle variation must be estimated with the goal of performing successfully the leg flight from back to front of the leg. Therefore an active swing angle of one fourth of the initial leg was purposed to be applied (see Table 4.1 and Figure 4.5).

In order to dimension the compliant parts of the leg it is important to estimate a geometric maximum retraction during stance. The dynamics of the systems are not simple, from Farley [56] considering the dog movement, the maximal leg retraction is limited by the geometry of the system, where the joint at point D (in Figure 4.3) must not touch the ground, which would imply $\beta_{attack} = \alpha_{leg}$. The maximal half-angle scan during stance of the virtual leg amounts to $\theta = 35°$ [56]. The angle of attack β_{attack} of the system can be estimated as:

$$\beta_{attack} = 90° - \theta \tag{4.19}$$

$$\beta_{attack} \geq 55° \tag{4.20}$$

The maximal spring contraction amounts occur during the swing phase, where the motor has to retract the leg more than it retracts itself during stance. It is assumed that a leg retraction exceeding by one forth the initial condition is sufficient to perform the flight of the leg, resulting in a $l_{\lambda,swing} = 0{,}6879$. In Table 4.1 is declared the angular variation theoretically predicted to the step cycle considering the mentioned assumptions.

4.1.2.2 Step cycle speed and gate characterization

In the leg locomotion of the telescopic leg, or the studied SLIP model from Seyfarth [60], it can be declared that the foot touches the ground with a non-zero horizontal velocity.

The state of the locomotion model is defined by the position $[x, y]^T$ and the velocity $\vec{v} = [v_x, v_y]^T$ at the point of mass at the hip joint. In the middle stance phase, where the maximum Δy is reached and is the point of vertical movement inversion, the $v_y = 0$, therefore, the system is fully described by v_x.

Farley [56] predicted a dynamic similarity where half the angle swept by the leg spring (θ, see Figure 4.4) is similar in animals of all sizes. Fallowing the values discussed the present project it will be assumed by estimation a θ of 20° which assign a β_{attack} of $70°$, fulfilling the requirement of an angle of attack greater than $55°$.

In this research, the time of foot contact was studied and extracted assessing the duration in the hip oscillation cycle. Assuming that the forward speed (v_x) is almost constant during the stance phase, the relationship between half the angle swept by the leg spring (θ) and the leg length L_0 allows obtaining the time of foot contact (t_c):

$$t_c = \frac{\sin\theta . 2L_0}{v_x} \quad [s] \tag{4.21}$$

To finalize this analisis of the step cycle angular variation, next is illustrated a table with the calculated values for the leg length and angles during the step cycle and the corresponding schematic graphic of the expected curve of the angle variation:

Step:	**Touchdown**	**STANCE** **16% retraction**	**SWING** **¼ retraction**
$\boldsymbol{l_{\lambda.}}$	0,917	0,770	0,688
$\boldsymbol{\varphi}$ **[degrees]**	130	94,908	79,321
$\boldsymbol{\alpha_{leg}}$ **[degrees]**	16,165	25,535	28,436
$\boldsymbol{\beta_{attack}}$ **[degrees]**	70	90	-

Table 4.1 - Leg length and angle variation during step cycle.

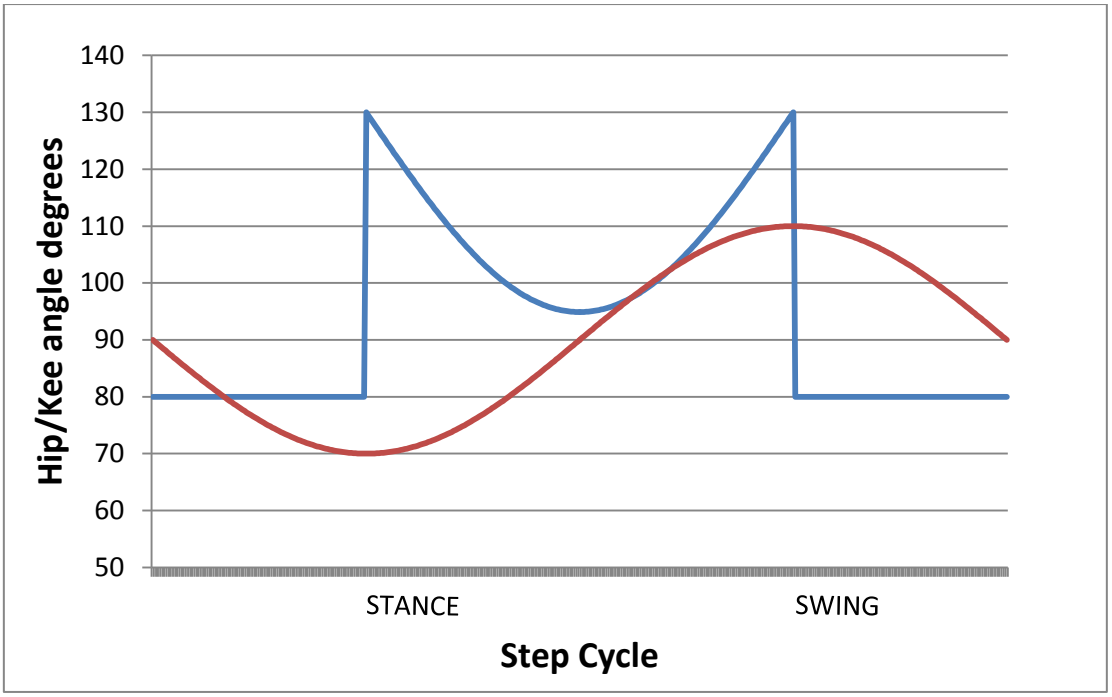

Figure 4.5 – Trajectory expected for the hip (red line) and knee (blue line) angles during the step cycle of 16%.

4.1.3 Weight factor

The weight factor has an important part in the study of the robot leg behavior. In autonomous walking robots there are important design requirement in terms of mass distribution which is a high challenging step [42].

As mentioned, it is considered the original predisposition of the trunk and head parts of the body of the Bioloid robot. For the legs, the three dimensional motion, and the orientation and assembly of the AX-12 servomotors, and the parts of the thigh segment of the leg from the knee joint upwards were maintained as the original model.

For the estimation of the weight and density of the new modeled components, in order to have a functional and robust performance, they cannot be equalized to the connective plastic parts of the robot nor the servomotors units (which hold the electronics at the thigh segment). To guarantee the cohesion and stability to the structure, considering the l_3 weight (of about 138 grams) the estimation adopted must be of about half of this mass for the l_1 new segment, which presents the same absolute length of l_3. With respect to the volume difference from l_1, the l_2 and l_4 segments weights are obtained by equivalence.

The different body parts weights of the robot have been assessed. The term "body part" is used to describe the sections in which the robot was divided. Afterwards, these values will be applied on Webots™ simulator world file [4].

Table 4.2 - Weight of the different body parts.

Part identification	Mass [g]
Trunk	692
Pelvis	170
Head	110
Neck	152
Leg $\boldsymbol{l_3}$ segment , $\boldsymbol{m_3}$	138
Leg $\boldsymbol{l_{2,4}}$ segment , $\boldsymbol{m_{2,4}}$	58 + 58 = 104
Leg $\boldsymbol{l_1}$ segment , $\boldsymbol{m_1}$	69

The robot total mass estimated is:

$$m_T = 4 \times (138 + 104 + 69)g\ [leg] + 692g[body] + 110g[head] + 170g[pelvis] + 152g[neck] = 2185\ g$$

In both trotting and running, at least two limbs are in contact with the ground at the same time, therefore in each leg the mean maximum mass estimation is $m_{MAX} = \frac{m_T}{2} = 1093g$, and the method of calculating k_{leg} gives the overall stiffness of the two limbs during ground contact [56].

4.1.4 Morphology for the Spring-Damping model

In the knee configuration, the mechanism can be reduced to a system with only one DoF simplifying the analysis and description of the global structures motion. It must be underlined that the linear equilibrium configuration is when the leg is extended (at touchdown) and that at half of the stance phase the leg reaches its most constrain point (see Figure 4.4).

The global equation for the motion in a linear spring-damp-mass model is:

$$m\frac{d^2x}{dt^2} + c\frac{dx}{dt} + kx = F \tag{4.22}$$

For the telescopic virtual leg as in a free undamped vibration system, the absence of force F and damping c, i.e., $F = c = 0$ for the equilibrium translation position:

$$m\ddot{\Delta L} + k_{leg}\Delta L = 0$$

With $x = \Delta L$

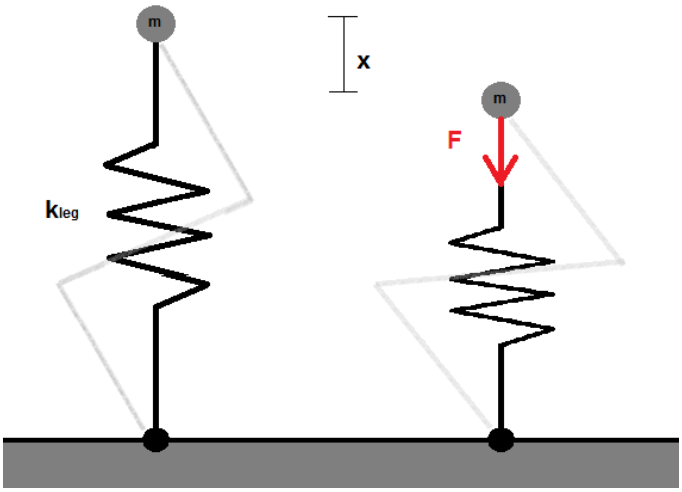

Figure 4.6 - Diagram of the virtual leg variation during retraction.

Thus, to generate compliant forces in the segmented leg it was introduced a virtual torsional spring of stiffness k_{spring} and damper with constant $c_{damping}$ at the inter-segmental joint, focused at point D (see Figure 4.3 and equivalent Figure 4.7) [52] [61] [62]. Following the previous linear concept, in case of an angular joint variation system the equivalent global equation of motion can be described by:

$$m\frac{d^2\theta}{dt^2} + c\frac{d\theta}{dt} + k\theta = T(\theta) \tag{4.23}$$

When the leg suffers this angle variation the spring at the knee joint acts as a restoring of the proportional force and the damper acts in the absorption of the velocities. In other words, the

spring possesses a relative high flexibility and is able to store the elastic energy opposing the applied force according to the respective spring stiffness coefficient k. On the other hand, the damper removes the energy from the elastic system taking into account the respective damping coefficient c, opposes the vibratory motion by consuming the mechanic energy [62] [63] [64].

The torque at the joint is proportional to the angle (for the spring torque) and angular velocity (for the viscous damping force) variation:

$$\tau(\varphi) = k_{spring}\Delta(\varphi) + c_{damping}\Delta(\dot{\varphi}) \tag{4.24}$$

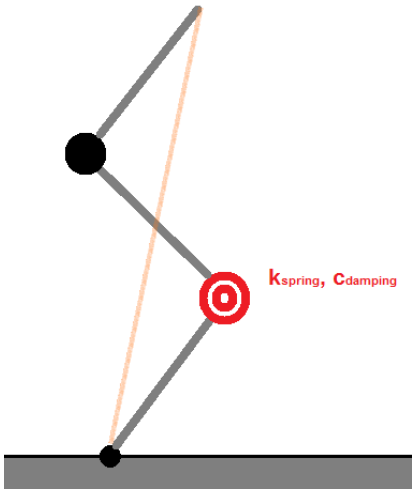

Figure 4.7- Schematic representation of the torsional spring and damping parallel system at the knee joint

Before, it was mentioned the desired retraction for the leg of 16% and the respective resulting variation of the knee angle. Thus, the $\Delta\varphi$ is already known however the velocity of this variation is still undetermined. From the time of stance phase previous reached and knowing the variation of the knee angle from the time of the touchdown to the middle-stance when the 16% retraction happens, the rotation speed at the joint may be calculated by:

$$\Delta\dot{\varphi} = \frac{\Delta\varphi}{t_c/_2} \tag{4.25}$$

Considering the application of a spring-damp system in point D as a compliant in the retraction during the walking and also the leg force due to the weight during locomotion at the virtual joint between segments 1 and 2/4, the resulting equation is:

$$l_{\lambda 1}.F_{leg}.\sin\alpha_{leg} = \frac{l_{\lambda 1}}{l_{\lambda 1}+\frac{l_{\lambda p}}{2}}.\tau(\varphi) \quad (4.26)$$

At this point all the kinematic foundation was settled and analyzed focusing on the study of the models configuration, e.g. the leg model lengths, segment orientations, velocities and forces for the step cycle and the implementation of the concepts is accomplished.

5 Experimental simulation

This chapter presents the Webots™ world model parameters and values, the physics plug-in needed to establish the pantograph mechanism as well as the controller features.

Here, the experimental procedures and assemblies are described. The quadruped compliant three-segmented leg modeling and simulation results are presented and ultimately a discussion on these is assessed.

5.1 Webots™ modelling

For the simulation is important to first introduce the quadruped, compliant leg system for the Bioloid robot. Main features are pantographic, three segmented, retractable, passive compliant legs. Also, the hip and knee joints are actuated using AX-12 servomotors mounted proximal, as well as the representation of the spring-damping system.

A world in Webots™ is a 3D description of the properties of robots and of their environment. It contains a description of every object: position, orientation, geometry, appearance, physical properties, type of object and others.

The proposed construction started from the world of Bioloid from Fillion-Robin [4] and the new adopted features were post-implemented in order to improve the legs performance. Therefore, most of the body's geometry was preserved and the elements were introduced in the world file as "pieces" of the new configuration taking into account the geometries and masses, according to the kinematic study with the goal of optimizing the effectiveness, leaving the appearance and aesthetics behind. Also, the main physical parameters such as weight and motor torque were taken from the original construction report of the Bioloid quadruped robot. Figure 5.1 shows the final quadruped robot model rendered in Webots™. A simplified and more readable release of the world file is also available in Appendixes A.

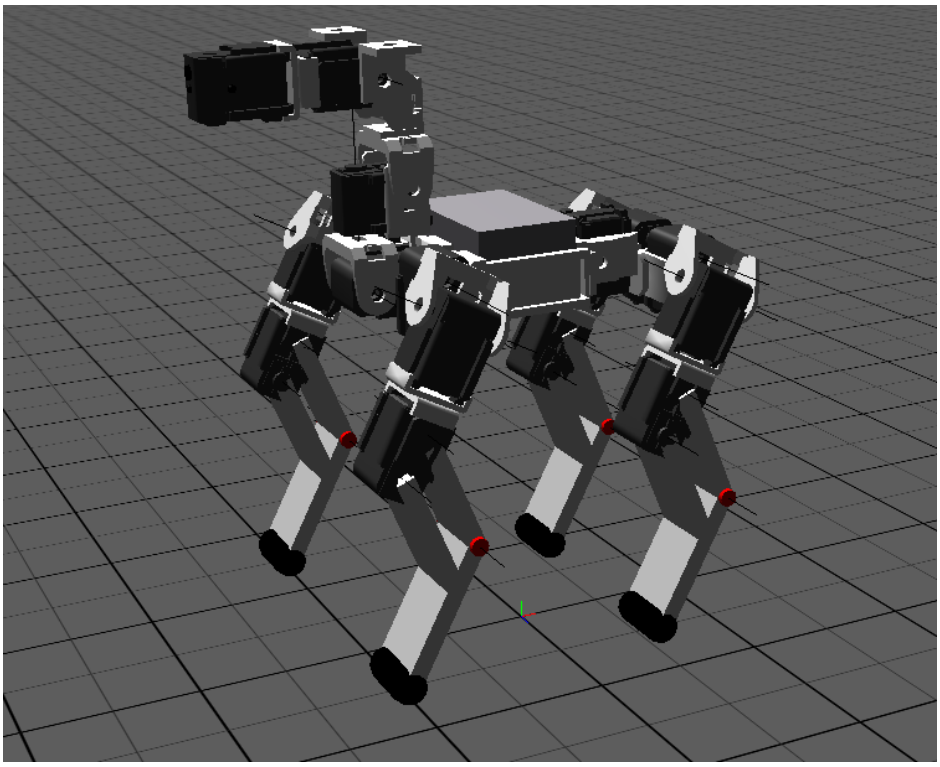

Figure 5.1 - New quadruped robot model rendered in Webots™.

5.1.1 Model Animation

The servo nodes are the links between the controller and the visual representation of the model used to add a joint (1-DoF) in a mechanical simulation. Giving orders to these servomotors, the Webots™ rendering engine is able to recompute the new position of the different joints, this way, the model is animated and can interact with the physics of the world.

The realism of the simulation can be achieved setting the parameters to the servo nodes, considering technical documentation for that (see section 5.3.1). For a better understanding of the servo influence, the different fields of the servo node are listed next in Figure 5.2.

```
Servo {
  SFString   type             "rotational"
  SFFloat    maxVelocity      10       # (0,inf)
  SFFloat    maxForce         10       # [0,inf)
  SFFloat    controlP         10       # (0,inf)
  SFFloat    acceleration     -1       # -1 or (0,inf)
  SFFloat    position         0
  SFFloat    minPosition      0        # (-inf,0]
  SFFloat    maxPosition      0        # [0,inf)
  SFFloat    minStop          0        # [-pi,0]
  SFFloat    maxStop          0        # [0,pi]
  SFFloat    springConstant   0        # [0,inf)
  SFFloat    dampingConstant  0        # [0,inf)
}
```

Figure 5.2 - Webots™ specification of the Servo node [65].

There are three different forces that can be applied in a servo joint: the motor force, the spring force and the damping force. The following fields can be specified:

- *maxForce*: specifies the default and upper limit of the motor torque/force, that is sent to the physics simulator to perform the requested motions. The documentation of the servo of AX-12 module gives a value is of 16.5 KgForce.cm which can be converted to 1.62 N.m [6] .
- *springConstant* and *dampingConstant:* allow the addition of spring and/or damping behavior to the joints, working in parallel as torsion elements on the rotation servo. These constant values must be specified as zero or positive. The default, zero value, will nullify the force/torque applied in the servo.

These three components can be switched on and off independently. According to the servo forces (Table 5.1), for the joint to obtain a passive spring & damper effect in the servo, the *maxForce* must be set to zero, which turns off the motor force, and the *springConstant* and *dampingConstant* to non-zero values [65].

Table 5.1 - Servo Forces [65].

Force	Motor Force	Spring Force	Damping Force
Turned on when:	maxForce > 0	springConstant > 0	dampingConstant > 0
Turned off when:	maxForce = 0	springConstant = 0	dampingConstant = 0
regular motor (the default)	on	off	off
regular spring & damper	off	on	on
damper (without spring)	off	off	on
motor with friction	on	off	on
spring without any friction	off	on	off

Considering the mechanical diagram of a servo represented in Figure 5.3, the servo is responsible for the joint linkage between two masses (m_0 and m_1), which is defined by the node in the parent on the servo by the Physics. An initial translation value is defined, x_0, and the variation of this position corresponds to x, as the current position.

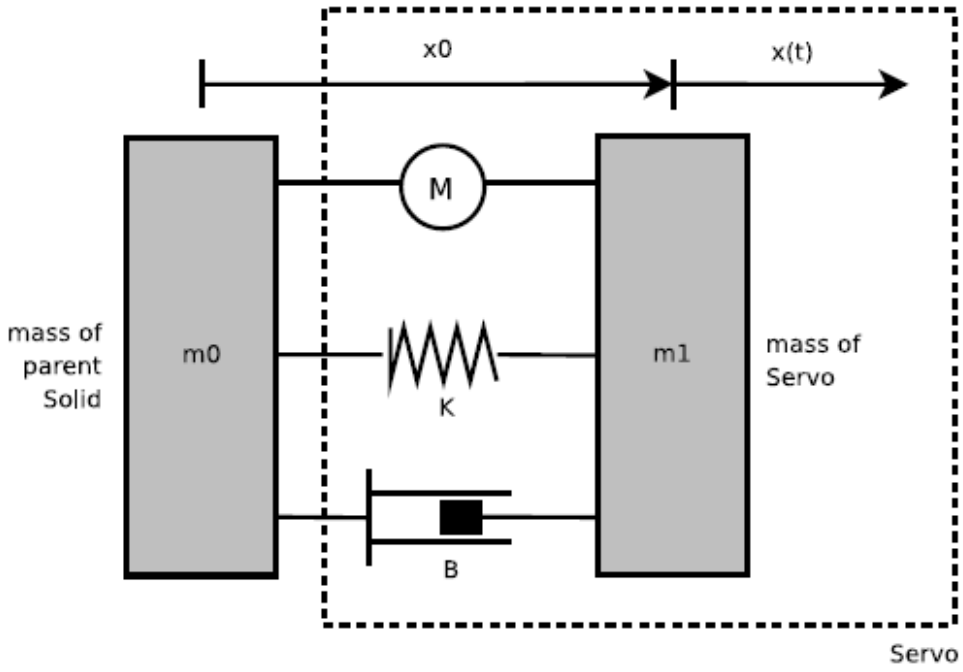

Figure 5.3 - Mechanical Diagram of a Servo [65].

Usually denoted as K, the *springConstant* field defines the value of the spring constant, also known as spring stiffness. The spring force is calculated according to Hooke's law:

$$F = K.\Delta x$$

where K is the *springConstant* and Δx is the variation from the initial position. Considering the application of springs in a robot, it is relevant to know the resting position for each servo which will correspond to the initial position of the servo.

The *dampingConstant* field specifies the value of the servo damping constant, represented as B in Figure 5.3. The damping torque/force is proportional to the effective servo velocity:

$$F = -B.v$$

where B is the damping constant and $v = \frac{dx}{dt}$ is the effective servo velocity computed by the physics simulator [4] [65].

The Webots™ enables the use of minimum and maximum stop values, which are the fields that specify the joints position of physical/mechanical stop that cannot be overrun by any force. However the use of this servo limits affects the passive functionality that is desired during the simulation and therefore they are not applied.

5.1.2 Servo Physics

The physical characteristics of any node derived from the *Solid* node to be used as physics parameter by the simulation engine are defined in the Physics node (Figure 5.4). An accurate model body dynamics need to match the ones of the real robot. It is important to establish the physical characteristics in order to perform an accurate simulation of the robot. The Webots™ simulator will apply the physics to all objects of the node hierarchy present between two servos.

```
Physics {
  SFFloat     density             1000      # (kg/m^3) -1 or > 0
  SFFloat     mass                -1        # (kg) -1 or > 0
  SFVec3f     centerOfMass        0 0 0     # (-inf,inf)
  MFFloat     inertiaMatrix       []        # empty or 6 values
  SFFloat     bounce              0.5       # [0,1]
  SFFloat     bounceVelocity      0.01      # (m/s)
  SFFloat     coulombFriction     1         # see ODE documentation
  SFFloat     forceDependentSlip  0         # see ODE documentation
}
```

Figure 5.4 - Webots™ specification of the Physics node [65].

In the kinematic analysis the values of the masses of the different parts of the robot were presented and, consequently, the total weight of the robot (see chapter 4.1.3) and the load hold by each member, considering the masses of the new additional parts on the legs of the robot Bioloid.

The center of mass (CoM) of the new body parts were set to be in the center of the components, once they are very symmetric and uniformly shaped and present internal equal weight. It is expressed in meters in the relative coordinate system of an X, Y, and Z location of the CoM with respect to the parental servo [4] [65].

5.1.3 Robot

The basis for building a robot is the Robot node which incorporates several fields, including specifications in terms of specifications applied to the controller, is presented in Figure 5.5:

```
Robot {
  SFString   controller         "void"
  SFString   controllerArgs     ""
  SFBool     synchronization    TRUE
  MFFloat    battery            []
  SFFloat    cpuConsumption     0    # [0,inf)
  SFBool     selfCollision      FALSE
}
```

Figure 5.5 - Webots™ specification of the Robot node [65].

A world file does not contain the controller code of the robots; the controller field must be filled with the name of the controller program that the simulator must use to control the robot. This program is located in a directory with the same name value. This directory is in turn located in the controller's subdirectory of the current project directory.

The controller specified in the world file, is written in another programming language supported by Webots™, the CodeBlocks which is a C++ IDE, operating across platforms, able to add functionalities by installing/coding a plugin [4] [65]. The code developed to insert in this section of the robot specification will be further mentioned in section 5.3.

5.2 Physics plugin

The physics plugin is a WebotsTM user-implemented shared library at run-time of the ODE physics engine. A physics plugin can be used, for example, to gather information about the simulated bodies, like the position, orientation or velocity, and/or to add forces, torques and extra joints to a simulation.

Webots™ itself was not able to reproduce the closed loop from the knee pantographic mechanism, so it had to be produced an ODE plugin to emulate it. The physics plugin created must be associated with the world file developed, therefore in the WorldInfo node the physics field was filled with the related name of the plugin.

For this work, due to the hierarchical setting of the servos in Webots™ modeling feature, the closed loop for the four joints presented in each pantographic construction demanded the addition of an extra joint to each leg to complete the mechanism intended. In more specific words, the parental connection between the thigh segment (link 3) and both shank segments (links 2 and 4) can be executed, however, the foot segment (link 1) cannot have two parental relationships with the mentioned shank links. Therefore for this goal, it was done the hierarchical linkage between l_1 and l_4 and an extra joint was created in the intersection of link l_1 with link l_2 (see Figure 5.6).

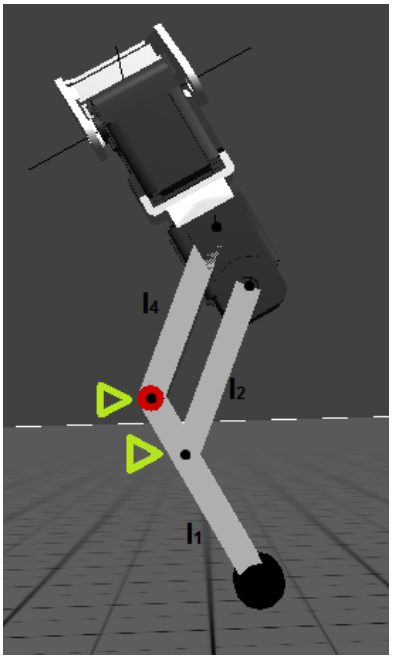

Figure 5.6 - Schematic representation of the extra joints to be added in the physics plugin (green down arrow l_1/l_2).

Throughout a plugin code implementation with adequate functions and interfaces it is possible to complete the pantographic mechanism at the middle joint, providing the physics for an accurate and reproducible simulation. This also requires that all controllers run in synchronous mode and must be set to TRUE (see Figure 5.5). The physics plugin developed for the implementation of a pantograph leg is described in Appendix B.

5.3 Locomotion control

First of all, it must be enlighten the operation of the locomotion intended for the model to perform. From the same process applied in the model developed by the Cheetah team [12] (mentioned in section 3.3.2) this project will settle on the same performance steps, using the leg model kinematics along with a compliant mechanism. These steps can be confined in three main operation modes at the joint: retracted position with actuated joint during swing, resting position with no actuation at touchdown and finally joint under external forces when it interacts with the ground. In terms of the spring-damping system actuation the spring equilibrium position extends at touchdown and becomes then gravity loaded during stance and actively retracted when the flight phase is ongoing.

5.3.1 Servomotor characterization

Before the control implementation it must be firstly known the servomotors features in order to accomplish the most reliable simulation by knowing the real characteristics of the robotic motor system that are being worked on.

The AX-12 module is a smart modular actuator, which incorporates a gear reducer that can produce high torque providing the necessary strength and resilience to withstand large external forces in the structure. Position and speed can be controlled with a high resolution (see Figure 5.7) [6] [4].

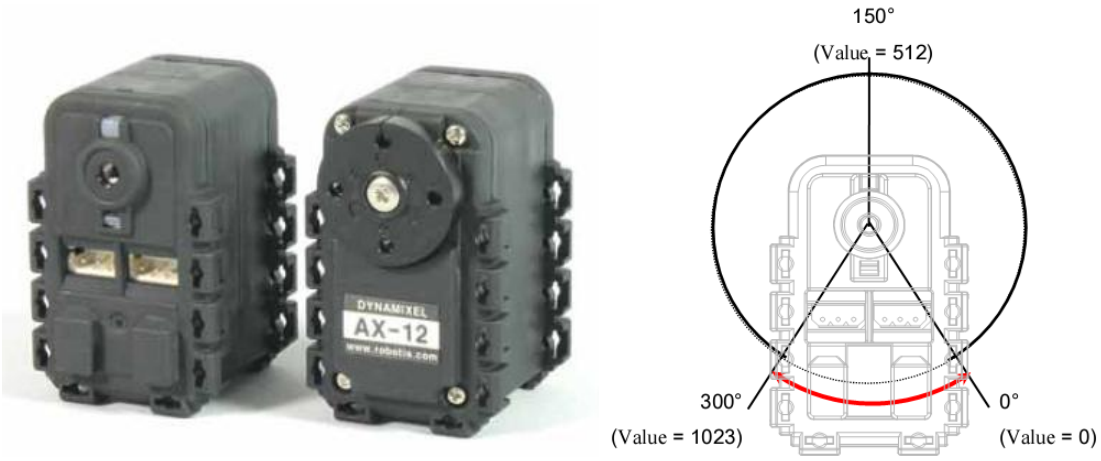

Figure 5.7 - AX-12 servomotors from Dynamixel and module rearview of actuation position [6].

These devices are chained together in series at the end of the controller, for both the data and for the power lines. As mentioned the controller can be programmed using a computer and a supplied program, CodeBlocks [9]. Each servomotor possesses an internal circuit responsible for the command interpretation. The details of the intercommunication are established taking into account the following characteristics:

Weight	55g
Maximum torque	16.5kgf.cm/ 1.62Nm (at 10V)
Maximum velocity	114 rpm
Maximum range of position	300°
Resolution	0.35°

Table 5.2 – AX-12 technical specifications [4] [6].

In Appendix C is presented the measurements of the AX-12 device, a complementary information about the servo, important in the segmentation study and regarding the design and assembly of the model's new parts (e.g. Figure 4.2)

5.3.2 Central Pattern Generator - CPG

The control foundation to be applied in the simulation brings the servomotors features together with the Control Pattern Generators (CPGs).

In animal locomotion, the signals produced to generate the sequences of muscular actuation can resemble the equivalent to CPGs located in the spinal cord as neural circuits that generate oscillatory output from a tonic input coming from the brain [4]. Therefore CPGs are highly diffused in the biologic research, becoming a very good tool due to the oscillator-network that is inherited. CPGs are oscillators responsible for the generation of movement throughout rhythmic pattern of neural activity, without necessarily receiving rhythmic input [4].

The frequent use of CPGs model in the locomotion control is due to a series of advantages comparing to the traditional methodologies. These generators are very robust, exhibit a limit cycle behavior, also show a simplified command at higher level with a reduced number of variables. Ultimately another advantage is the really good basis for learning and optimization algorithm [11] [12].

Knowing the principles of work of CPGs and concepts of cyclic and rhythmic motion during locomotion behavior these oscillators come as adequate option for the control of the Bioloid quadruped robot. The controller implemented was an adaptive improvement of a template previously provided by Vitor Matos, a PhD researcher at Control, Automation and Robotics Group of the University of Minho.

5.4 Simulation

At this point the model is finalized and the desired operation control is implemented. For the Bioloid quadruped with CPG control, the hip joints are modeled as normal angular motors with a rhythmic oscillatory actuation. On the other hand, for the knee joint mechanism which is achieved through a physics plugin to complete the pantographic construction, is adopted a condition to control the compliant joints. The control of the middle-leg joint consists in two main steps. The first is when the flight phase is ongoing that the joint is actively retracted to avoid the impact with the ground and consequently the stumble and fall of the robot. The stance phase corresponds to the second step where the motor force is off, i.e. the servomotors are now non-actuated and the *springConstant* and *dampingConstant* attributes are on and are the two only forces actuating in the joint.

For the simulation the input implemented for the hip and knee angles were the ones studied in the previous chapters and described in Table 4.1 and Figure 4.5 and the main commands are described in Appendix D for the input signals of the controlling servos. Therefore, the angles activity and development during simulation is the focus of study and the target of analysis.

5.4.1 Analysis of the quadruped behavior

Running the simulation allows access to the performance of the implementations done in the new quadruped leg mechanism. Simulating the quadruped robot walking is a very complex task. The goal was for the Bioloid execute a 16% retraction when the contact with the ground happens.

Compliance behavior has long been demonstrated to improve robot walking over uneven surfaces. Using a spring as a force element also allows torque control by controlling the deflection of the spring. The use of damping in combination with the spring is expected to improve stability under compliant control. High damping is desirable for more precise foot placement but leads to higher energy losses during stance, and vice versa [66] [67].

Thus, before proceeding to more deepen experimental simulation, it was carried out an evaluation of the performance of the spring and damping coefficients to secure applicable limitation values maintaining structural stability and without physical disassembling. From this short study it was possible to extract that high coefficient of damping or a coefficient of damping greater than spring are not good, due to the fact that the world file would “explode”, i.e. there the ODE does not respond to the differential equation, therefore the locomotive motion is not possible. Also, the use of only a spring in the knee articulation shows high levels of vibration, and extremely high values also disassemble the mechanism.

Hutter [68] studied the benefit of high rigid spring in combination with low damping. This configuration allows storing and releasing a substantial amount of energy during ground contact phases. These principles were adapted from nature taking into account the tendons and elastic elements in muscles. This approach showed a significant energy benefit and in the power consumption of the actuators in highly dynamic maneuvers. Approximately 20% of the total energy is inserted by the motor while the rest is created passively.

The previous kinematic study together with this independent study of the applicable values of the compliant elements at the joint, allowed the estimation of the spring and the damping values in order to maintain the consistency and requirements of the model. Thus, considering a reasonable range of values for the compliant model a series of simulation studies were performed. There were settled five spring constant values $[0.5;\ 1.0;\ 1.5;\ 2.0;\ 2.5\ \mathrm{N.m/rad}]$ and four co-working damping constants $[0.01;\ 0.015;\ 0.02;\ 0.025\ \mathrm{N.m.s/rad}]$ in order to study the variation of the knee angle during motion.

For the study of the behavior of the spring-damp model coupled with the controller it was performed the study without the floor contact. In other words, to study if the intended movement at the joints and the synchronization with the controller, the external forces were excluded and the angle variation was evaluated.

In this section is examined the performance for considering two specific cases, when the spring constant is fixed to $1.0\ \mathrm{N.m/rad}$ and when damping constant is fixed to $0.02\ \mathrm{N.m.s/rad}$. For an extensive consult of all the simulation cases in Appendix E is displayed the joints angles performance of each simulation.

First, for the analysis of the behavior of the leg knee angle variation during simulation for the front left leg of the Bioloid is graphically represented in Figure 5.8, comparing the theoretical values expected with the Webots™ simulation values for the different damping constants when the spring constant is fixed to $1.0\ \mathrm{N.m/rad}$. For the remaining legs, the output signals were similar.

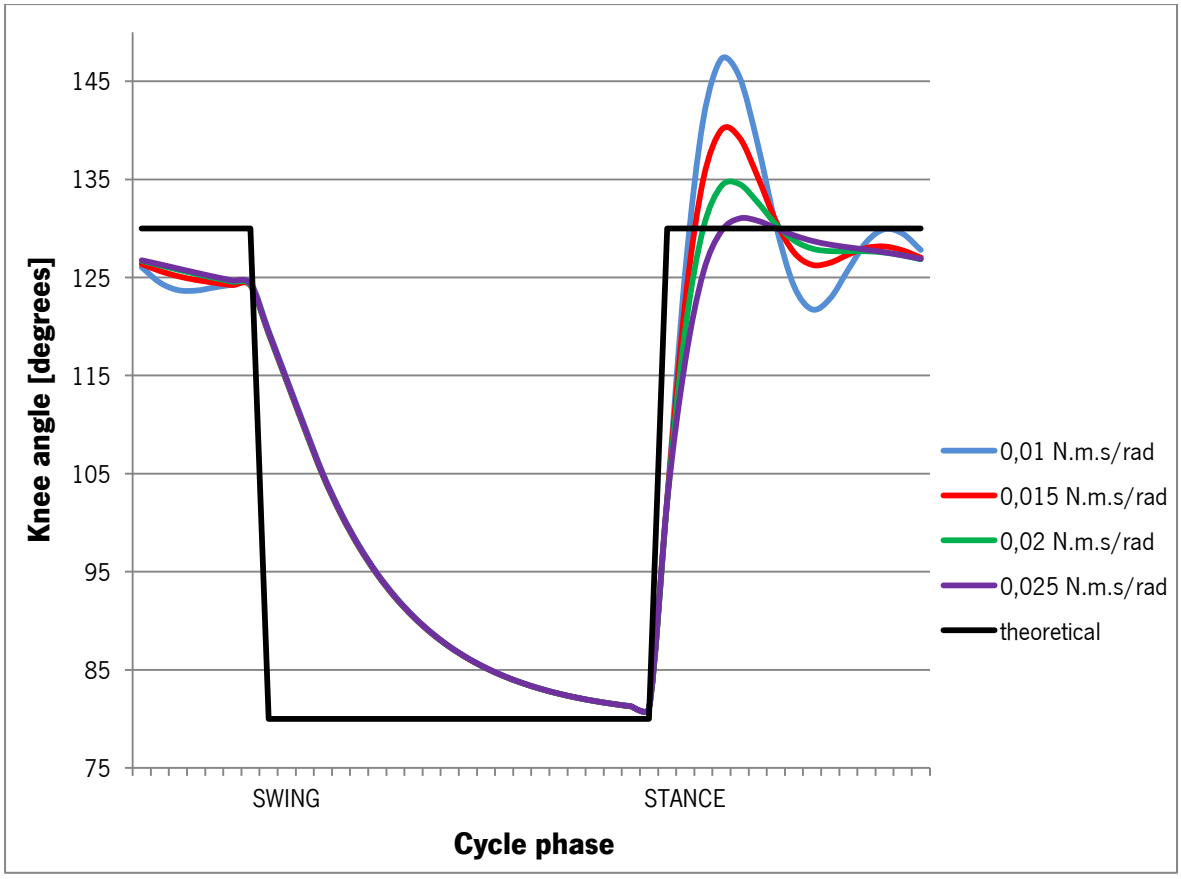

Figure 5.8 – Simulation trajectory of the theoretical (black line) and practical knee angles during the step cycle with spring constant of 1.0 N.m/rad for different damping constant values.

By observation of the several simulations performed (e.g. Figure 5.8) it can be observed a similar retraction process during swing phase. Therefore for the study of the performance of the spring-damp model behavior the further analysis is focused in the transition from swing to stance, which corresponds to the point when the model acts passively and the forces perform self-sufficiently. The Table 5.3 shows the mean deviation of the simulation at the swing-to-stance point of the knee angles for the different damping constants when the spring constant is fixed to $1.0\ \mathrm{N.m/rad}$.

Table 5.3 – Mean deviation at the swing-to-stance point of the knee angles during the step cycle with spring constant of 1.0 N.m/rad for different damping constant values.

Damping constant: [N.m.s/rad]	**0,01**	**0,015**	**0,02**	**0,025**
Mean deviation	3,93	3,187	2,811	2,815
% deviation	3,023	2,452	2,162	2,165

For a further analysis of the spring behavior when is fixed the damping coefficient is presented next a graphical representation for a damping constant of $0.02\ \mathrm{N.m.s/rad}$ the different curves of the knee angular joint for the different spring constants:

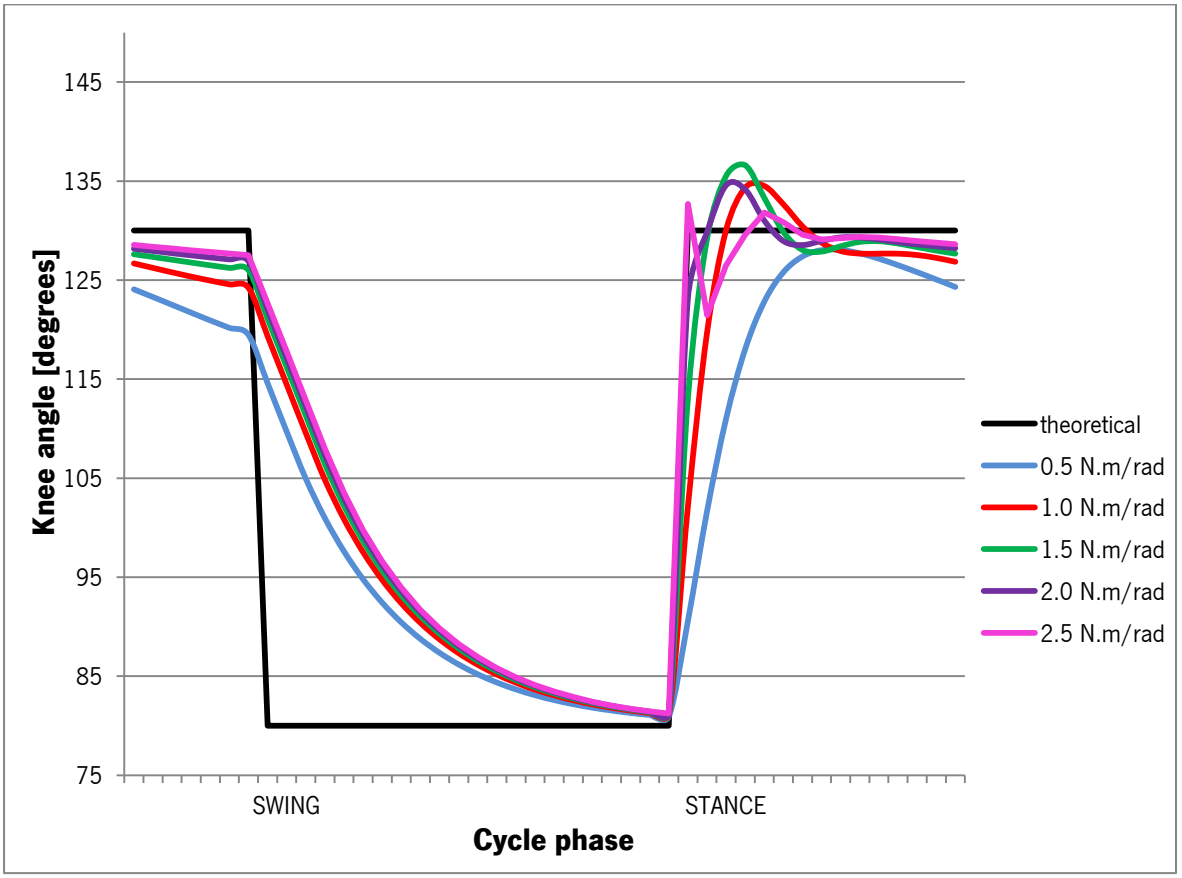

Figure 5.9 - Simulation trajectory of the theoretical (black line) and practical knee angles during the step cycle with damping constant of 0.02 N.m.s/rad for different spring constant values.

And the corresponding results of the mean deviation for the simulation at the swing-to-stance point of the knee angles for the different spring constants when the damping constant is fixed to $0.02\ \mathrm{N.m.s/rad}$ are presented in the next table:

Table 5.4 - Mean deviation at the swing-to-stance point of the knee angles during the step cycle with damping constant of 0.02 N.m.s/rad for different spring constant values.

Spring constant: [N.m/rad]	**0,5**	**1,0**	**1,5**	**2,0**	**2,5**
Mean deviation	5,591	2,811	1,767	1,019	0,973
% deviation	4,301	2,162	1,359	0,784	3,429

5.5 Results discussion

In summary, for the experimental simulation the main goal was to perform a walking operation as simple and consistent as possible. For the leg modeling design basic considerations are able to be outlined: the leg end point trajectory should lie on a straight-line; the leg must show a simple mechanical design; and for last the leg should ensure suitable motion capability. The combination of these requirements in a new model of a mammal-like three-segmented leg design for Bioloid, featuring a pantograph mechanism that ensures parallelism between two of the three leg segments and help keeping the number of degrees of freedom low, results in a major mechanical advantage.

With regard to the controlling of the joints motion, an important enhancement to a stable locomotion is the implementation of an active retraction at the leg knee. Ultimately, the addiction of a passive compliant system was inherited, with dimensioned leg stiffness and damping, performing the mentioned operation progression in a locomotion simulation study.

As mentioned before, the angles activity during simulation is the focus of study and the target of analysis. The hip joint performs a continuous and active motion during the simulation with amplitude of 20° as commanded.

Differently from the hip, in the knee compliant joint analysis is expected a nonlinear behavior due to different operation modes adopted by the joint during the step cycle and also due to different values of spring-damp coefficients applied in the simulations.

Throughout the analysis of the several studies, it can be concluded that after the lift-off point of the quadruped's foot, when it starts the swing phase, the active retraction in all the simulations is not instantaneous, on the contrary, it takes a certain time to conclude de 50 ° variations. However, the slow velocity of performance at this point is not an issue, because the retraction goal is to flight the leg without impact with the ground and this task is achieved.

From the observation of Figure 5.8 and the consulting Table 5.3 it can be inferred that for the spring constant value of $1.0\ \mathrm{N.m/rad}$ the lowest deviation of the goal performance at the knee joint is for higher values of damping.

Through deeper observation of the different study cases it can be declared that the spring at the point of phase shift from swing-to-stance also has the function of quickly reset the touchdown position. Analyzing the performance of the knee joint when the damping coefficient is fixed and the spring coefficient is changed, in Figure 5.9, it can be inferred that for greater spring values the efficiency in resetting the touchdown position is increased.

Generalizing, from the simulations performed it can be assessed that the spring has the function of extend the leg and maintain its length during the stance phase. In turn, the damp component plays a role in the avoidance of oscillations acting in the reduction of the vibration at the joint.

Respective values of the mean deviation for the simulation at the swing-to-stance point of the knee angles for the different spring and damping constants are presented in the Table 5.5 and corresponding graphic schematization, Figure 5.10:

Table 5.5 – Mean deviation at the swing-to-stance point of the knee angles during the step cycle as function of the spring and damping constant values.

Spring constant: [N.m/rad]	Damping constant: [N.m.s/rad]	**0,01**	**0,015**	**0,02**	**0,025**
0.5	**Mean deviation**	6,332	5,462	5,591	6,295
	% deviation	4,871	4,202	4,301	4,843
1.0	**Mean deviation**	3,93	3,187	2,811	2,815
	% deviation	3,023	2,452	2,162	2,165
1.5	**Mean deviation**	2,577	2,123	1,767	1,713
	% deviation	1,982	1,633	1,359	1,318
2.0	**Mean deviation**	2,449	1,332	1,019	1,176
	% deviation	1,884	1,024	0,784	0,905
2.5	**Mean deviation**	1,579	1,261	0,973	2,004
	% deviation	1,215	0,97	0,749	1,541

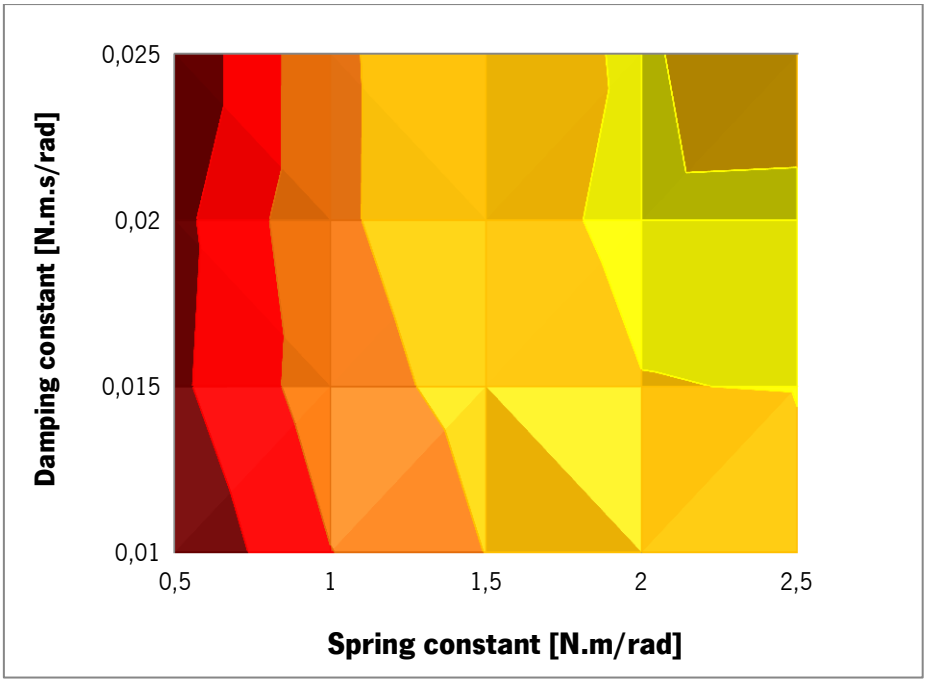

Figure 5.10 - Mean deviation at the swing-to-stance point of the knee angles during the step cycle as function of the spring and damping constant values.

From the evaluation of the performances of the different spring-damp coupled coefficients shown (see Appendix E), it can be determinate that spring constant values over $1.5\ \mathrm{N.m/rad}$ the phase transition is done faster and more efficiently. However for k values over $2.5\ \mathrm{N.m/rad}$ in spite of the success in the achievement and preservation of the knee extended angle during stance the spring force is too high and "explodes" at the model's middle joint, which disintegrates due to inappropriate values in the physics engine.

The increasing of spring constant values forces the introduction of greater damping constant values is required due to the fact that the high spring constants presents larger vibration forces to be suppressed. When is applied low spring values and high damp coefficients (e.g. $\mathrm{k} = 0.5\ \mathrm{N.m/rad}$ and $\mathrm{c} = 0.025\ \mathrm{N.m.s/rad}$) the extension of the leg is not complete, therefore at the touchdown the leg is not ready to support the weight of the robot.

Ultimately, it must be underlined that the use of spring and damping components in Webots™ is a very complex task, it is very difficult to mimic a real muscular application in the present mechanism. Mentioned studies [68], follow the concept of the application of higher spring values co-working with lower damp constants and in the leg model of this project shows an according satisfactory conduct with that concept.

It must be found a structural and dynamic equilibrium between the applicable values of the spring and damping coefficients, the weight and the controller of the robot in order to obtain a synchronized, balanced and consistent walking quadruped.

At this point, after the observation of the spring and damping constants applied in the model, it can be extracted the more appellative values to use for a locomotion with contact with the ground. However, when the simulation is played there is a balance issue that prevents the robot to accomplish a successful locomotion.

Due to the major problem of imbalance of the robot, there are several considerations that must be taken into account to solve this issue. First is the active equilibrium of the robot, in which the controller has the main part. The actuation of the servomotors must be coordinated and engaged with the passive components at the robots joint. Secondly, following the animal behavior, the back part of the robot can present a light increase in the mass contributing also for the robot equilibrium. Also mimicking the mammal-quadrupeds like the dog, the crouched position may be a good option to resolve this issue. This last method is an answer being applied in other researching studies.

The use of more crouched postures brings a slightly shorten back leg segment and consequently the angles also change. The different relative leg lengths may come as an important step to help in the stability of the Bioloid as well as the robot similarity to the animal behavior. Taking the crouched inspiration of small mammals [11] [49], the design adapts the configuration differently, i.e, the back legs design must be of 20% shorter than the frontal legs.

6 Conclusions and future work

This last chapter presents the main conclusions withdraw from the work carried out, exposing some suggestions to a future development in order to complement the results and criteria for a real robotic implementation.

6.1 General conclusions

This project aim is the design of a new leg model to be implemented in the Bioloid quadruped robot in order to perform a stable and linear locomotion, taking inspiration from nature and following previous studies principles. To begin with, the goal is to achieve a real assembling of the developed mechanism, for such, the objective was to achieve a stable simulation of the novel quadruped using appropriate virtual software.

For a proper foundation for the new design and before the practical model implementation and experimentation itself, it was done a study of the legged machines and robotic mechanisms already developed by researchers and a state-of-the-art concerning the passive compliant mechanisms in leg joints applied in the past few years. From this study it was verified that the compliance implementation in locomotion systems shows positive outcomes in the stability and impact neutralization.

The robotic leg mechanism structure is the focus of the modeling section. A study of the pantographic configuration was conducted and a deepen approach was taken considering the Cheetah design. This robot has proven to be of great interest in both fields of model structure characteristics and also in the operation of the compliant leg. The concepts of the pantographic structure were clarified and optimized to the application in the legs modeling and the operation modes are a major contribution for the simulation control during locomotion. The pantographic design is advantageous since it completely avoids structural instability maintaining the basis of leg segment configurations observed in nature.

In this perspective, centering the work in the configuration of the leg, a fair amount of parameters must be taken into account: the lengths and orientation of the limb segments, velocities and forces during step cycle and the localization and configuration of the compliant elements (in this case a virtual torsional spring-damp model). Therefore, a kinematic study of the rotation in the leg's joints was conducted and consequently the dimensioning of the compliant system introducing a simple virtual torsional spring-damping model. It must be underline that the leg segment lengths were chosen to be energetically advantageous. Taking into account these measurements, further calculations allow an estimation of the leg length during a complete step cycle, thus, defining the required leg length range and the forces in play.

At this point the modulations of a world file in Webots™ of the new components to integrate into the mentioned new mechanism needed to simulate the Bioloid robot, are the next step. With proper setting, the physics plugin realistically emulates the real robot's leg's behavior, giving consistency to the pantographic assemble as well as the control system based on Control Pattern Generators allowing a harmonic and rhythmic locomotion to the quadruped, which proved to be one of the biggest challenges in building the simulation.

For the controlling implementation, the hardware servos were characterized. Both hip and knee joints were actuated by using the same AX-12 motors. The requirements here were to avoid using complex physics and activity in the simulation, but still have a behavior of the legs close to reality. In order to achieve these goals, a CPG based supervisor provided by Vitor Matos had to be improved and furthermore implemented in the assembly.

Finally, all the parts were assembled and the leg is ready to be tested. The locomotion simulating of the quadruped robot walking is a very complex task. As one main goals of the project was to try to characterize the compliant system evaluating the performance of the joints activity, at the hip and knee, exported to a MATLAB algorithm and the results were able to be observed and discussed.

Primarily, the experiments were developed without the floor contact excluding the influence of external forces. In all the testes performed the hip joint performs the expected continuous harmonic motion with amplitude of 20°.

At the spring-damping models it was applied a close range of values and evaluated the outcome behavior during leg motion. First it was performed an independent study from each of the components spring and damping applicable in the model maintaining the structural stability and cohesion achieving the physical limit values of the coefficients. Thus, contrary to the hip, the behavior at the knee joint was varied for the several experiments. The main variation happens during stance, i.e. during the swing phase the joint is actuated and its performance is similar in all the simulations reaching the goal of flight the leg. Focusing on the development of the activity at the knee joint during stance, results show that the robots leg behaved better when the spring values are around $2.0 - 2.5\ \mathrm{N.m/rad}$ and corresponding $0.02\ \mathrm{N.m.s/rad}$ of damping coefficient. For this values, at the point from swing-to-stance and touchdown the deviation from the theoretical values are the lowest, presenting best performance in the resetting and maintenance of touchdown and position with the lowest vibration results.

From the no-contact study it would be possible to implement the results in normal walking experiments however, the model does not present a balanced locomotion being impossible to assess the behavior of the joints when the ground force is in place. It must be found a structural and dynamic equilibrium between the applicable values of the spring and damping coefficients, the weight and the controller of the robot in order to obtain a synchronized, balanced and consistent walking quadruped.

6.2 Future work and final remarks

Throughout the work herein described, there were some limitations that prevented the detailed study of some aspects. There are several improvements that should be deepened in order to obtain a further developed model.

An incomplete task was the realization of a stable and balanced locomotion by the quadruped robot. There are three main solutions that should be taken into account in order to resolve this issue.

The first, and with a major influence on this matter is the actuation of the servomotors controlling system, which may be improved to obtain a more accurate and synchronized gate motion. The simplicity of the control of this system limits the study of the quadruped gate. The development of an actuation to apply slower or faster walks may come as a benefit to amplify the locomotion study of Bioloid gate. Also, the use of sensors feedback in the actuation control, as a imitation of the central nervous system in animals, may come as an advantage by promoting the interaction between the environment and the machine, helping in the guidance and retraction of the quadruped movement through obstacle and ground force detection respectively.

A second solution to improve the robots performance may arise from the mass redistribution. Following the dog physiology the hind legs can show a slight increase in the weight contributing also for the robot equilibrium. Also, it may be considered the materials applied in the new model parts as well in the electronics, influencing the total weight of the robot and consequently the balance during the locomotion.

Following the pattern of mimicking animal locomotion the crouched position design is a method applied in some researching studies and shows potential to improve the locomotion unbalance. The posture of the crouched design presents different configuration of the frontal and distal limbs in terms of length and angles. In other words this method presents a slightly shorter back leg which improves the stability of the Bioloid.

The model would greatly benefit from more extensive calibration experiments, particularly with regard to the knee-joint mechanism taking into account the spring-damping system for different gates. The deepen knowledge about the behavior of the compliant mechanism in the joint

can also be converted in an algorithm that adapts the leg for the different velocities that the Bioloid robot may present.

Another major improvement could be achieved by implementing a forth segment to the leg, corresponding to the toe segment providing also an extra compliant element to the leg as well as more stability. This compliant system would work passively as a support unit in the retraction of impact during gate. For instance, the use of a rubber band around the axis is an easy implementation, where its elastic properties helps to dampen the touchdown impact and also restitutes some of its energy at takeoff.

Ultimately, there is also the improvement of the appearance and aesthetics of the model to perhaps a more advanced animal-like look.

7 Bibliographic References

[1] E. Ottaviano, S. Vorotnikov, M. Ceccarelli and P. Kurenev, "Design improvements and control of a hybrid walking robot," vol. 59, p. 128–141, 2011.

[2] M. H. Raibert, "Legged Robots that Balance," *Communications of the ACM,* Vols. 29-6, 1986.

[3] G. Carbone, A. Yatsun, M. Ceccarelli and S. Yatsu, "Design and Simulation of Cassino Hexapod Robot," in *ICS'09 Proceedings of the 13th WSEAS International Conference on SYSTEMS*, Wisconsin, USA, 2009.

[4] J. Fillion-Robin, "Modeling of a real quadruped robot using WebotsTM simulation platform," School of Computer and Communication Sciences - EPFL, Switzerland, 2007.

[5] F. Wyffels, M. D'Haene, T. Waegeman, K. Caluwaerts, C. Nunes and B. Schrauwen, "Realization of a passive compliant robot dog," in *Proceedings of the 2010 3rd IEEE RAS & EMBS International Conference on Biomedical Robotics and Biomechatronics*, Tokyo, Japan, 2010.

[6] Dynamixel AX-12 - User Manual, Robotis, 2006.

[7] R. Oliveira, "Desenvolvimento de Plataforma de Investigação em Robôs Humanóides Autónomos," Instituto de Sistemas e Robótica - Instituto Superior Técnico, 2010.

[8] R. Oliveira and R. Ventura, "Development of a Computing Platform for the Bioloid Humanoid Robot," 2010.

[9] A. Mensink, "Characterization and modeling of a Dynamixel servo," University of Twente - EEMCS / Electrical Engineering, The Netherlands, 2008.

[10] M. M. Williamson, "Series Elastic Actuators," Master's thesis, Massachusetts Institute of Technology, Cambridge, MA , 1995.

[11] S. Rutishauser, A. Spröwitz, L. Righetti and A. Jan Ijspeert, "Passive compliant quadruped robot using central pattern generators for locomotion control," 2008.

[12] A. Tuleu, "Improvement of the Cheetah Locomotion Control," École Polytechnique Fédérale de Lausanne, Lausanne, Switzerland, 2010.

[13] M. Riess, "Development and Test of a Model for the Cheetah Robot," Biologically Inspired Robotics Group - EPFL, Lausanne, 2008.

[14] I. Kviatkevitch, "Locomotion exploiting body dynamics on the Cheetah robot," wiss Federal Institute of Technology Lausanne, 2009.

[15] R. Van Ham, T. Sugar, B. Vanderborght, K. Hollander and D. Lefeber, "Compliant Actuator Designs. Review of Actuators with Passive Adjustable Compliance/Controllable Stiffness for Robotic Applications.," vol. 16/3, p. 81 – 94, 2009.

[16] L. Visser, R. Carloni, R. Unal and S. Stramigioli, "Modeling and Design of Energy Efficient Variable Stiffness Actuators," Alaska, USA, 2010 .

[17] B. Vanderborght, T. Sugar, R. Van Ham, K. Hollande and D. Lebefe, "Comparison of mechanical design and energy consumption of adaptable, passive-compliant actuators," 2008.

[18] B. Vanderborght, N. G. Tsagarakis, C. Semini, R. Van Ham and D. G. Caldwell, "MACCEPA 2.0: Adjustable Compliant Actuator with Stiffening Characteristic for Energy Efficient Hopping," Japan, 2009.

[19] M. Laffranchi, H. Sumioka, A. Sproewitz, D. Gan and N. G. Tsagarakis, "Adaptive Modular Architectures for Rich Motor Skills - Compliant Actuators," Italian Institute of Technology, 2011.

[20] N. G. Tsagarikis, A. Jafari and D. G. Caldwell, "Novel Variable Stiffness Actuator: Minimizing the Energy Requirements for the Stiffness Regulation," Italy, 2010.

[21] K. Hollander, T. Sugar and D. Herring, "Adjustable robotic tendon using a 'Jack Spring'," USA, 9th International Conference on Rehabilitation Robotics, 2005, pp. 113 - 118 .

[22] B. Vanderborght, R. Van Ham, M. Van Damme and D. Lefeber, "Using Compliant Actuators in the Mechanical Design of Robots developed at the VUB," Belgium, 2010.

[23] C.-P. Chou and B. Hannaford, "Measurement and modeling of McKibben pneumatic artificial muscles," USA, IEEE Transactions on Robotics and Automation, 1996.

[24] B. Vanderborght, B. Verrelst, R. Van Ham, M. Damme, D. Lefeber, B. Duran and P. Beyl, "Exploiting Natural Dynamics to Reduce Energy Consumption by Controlling the Compliance of Soft Actuators," in *The International Journal of Robotics Research*, 2006.

[25] S. A. Migliore, E. A. Brown and S. P. DeWeerth, "Biologically inspired joint stiffness control," in *Proc. 2005 IEEE International Conference on Robotics and Automation.*, Laboratory for Neuroengineering, Georgia Institute of Technology, Atlanta, Georgi, April 2005.

[26] J. W. Hurst, J. E. Chestnutt and A. A. Rizz, "An Actuator with Mechanically Adjustable Series Compliance," USA, Robotics Institute, 2004.

[27] J. C. J. a. R. A. Hurst, "An Actuator with Physically Variable Stiffness for Highly Dynamic Legged Locomotion.," in *Proc. of IEEE International Conference on Robotics and Automation*, New Orleans, LA, USA, April 2004.

[28] J. W. Hurst, J. E. Chestnutt and A. A. Rizzi, "The Actuator With Mechanically Adjustable Series Compliance," vol. 26, USA, IEEE Transactions on Robotics, 2010.

[29] T. G. Sugar, "A novel selective compliant actuator," *Mechatronics Journal,* vol. 12, p. 1157–1171, November 2002.

[30] J. Pratt and B. Krupp, "Design of a bipedal walking robot.," in *Proceedings of the SPIE*, USA, 2008.

[31] S. Au and H. Herr, "On the design of a powered ankle-foot prosthesis: The importance of series and parallel motor elasticity," *IEEE Robotics and Automation Magazine,* 2008.

[32] J. Pratt and G. Pratt, "Intuitive control of a planar bipedal walking robot," in *IEEE Int. Conf. Robotics and Automation*, Belgium, 1998.

[33] J. W. Hurst, J. E. Chestnutt and A. A. Rizzi, "Design and Philosophy of the BiMASC, a Highly Dynamic Biped," Pennsylvania, USA, IEEE International Conference on Robotics and Automation, 2007.

[34] P. Beyl, B. Vanderborght, R. Van Ham, M. Van Damme, R. Versluys and D. Lefeber, "Compliant Actuation in New Robotic Applications," in *Proceedings of the NCTAM06 - 7th National Congress on Theoretical and Applied Mechanics*, Mons, Belgium, May 2006.

[35] B. Vanderborgh, B. Verrelst, R. Van Ham, M. Van Damme, P. Beyl, and D. Lefeber,

"Development of a compliance controller to reduce energy consumption for bipedal robots," *Autonom. Robots,* vol. 24, p. 419–434, 2008.

[36] C. Tavolieri, E. Ottaviano, M. Ceccarelli and A. Nardelli, "A Design of a New Leg-Wheel Walking Robot," in *Proc. of 15th Mediterranean Conf. on Control and Automation*, Athens, Greece, 2007.

[37] C. Tavolieri, E. Ottaviano, M. Ceccarelli and A. Nardelli, "Analysis and Design of a 1-DOF Leg for Walking Machines," in *Proceedings of RAAD'06, 15th International Workshop on Robotics in Alpe-Adria-Danube Region*, Cassino, Italy, 2006.

[38] E. Ottaviano, M. Ceccarelli and C. Tavolieri, "Kinematic and Dynamic Analyses of a Pantograph-Leg for a Biped Walking Machine," *7th CLAWAR,* pp. 561-568, 2004.

[39] W. C. Yuen, "Robust Walking of a Quadruped Robot," Master Thesis, National University of Singapore, Singapore, 2004.

[40] C. Liang, M. Ceccarelli and Y. Takeda, "Operation Analysis of a One-DOF Pantograph Leg Mechanisms," *Proceedings of 17th International Workshop on Robotics in Alpe-Adria-Danube Region,* 2008.

[41] R. Pfeifer, M. Lungarella and F. Iida, "Self-Organization, Embodiment, and Biologically Inspired Robotics," *Science,* vol. 318, 2007.

[42] D. C. Kar, "Design of Statically Stable Walking Robot: A Review," *Journal of Robotic Systems,* p. 671–686, 2003.

[43] J. Z. Kolter, M. P. Rodgers and A. Y. Ng, "A Control Architecture for Quadruped Locomotion Over Rough Terrain," in *IEEE International Conference on Robotics and Automation*, Pasadena, CA, USA,, 2008.

[44] F. Delcomyn and M. E. Nelson, "Architectures for a biomimetic hexapod robot," *Robotics and Autonomous Systems,* vol. 30, p. 5–15, 2000.

[45] T. Zielinska and J. Heng, "Mechanical design of multifunctional quadruped," *Mechanism and Machine Theory,* vol. 38, p. 463–478, 2003.

[46] A. Deshmukh, "Robot Leg Mechanisms," *Department of Mechanical engineering - Indian Institute of Technology,* 2006.

[47] O. Lenord and J. Albiez, "Improvement of biologically inspired quadrupedal walking strategies using computational multibody dynamics," in *Proceedings of the Multibody Dynamics*,

Lisbon, Portugal, 2003.

[48] H. Witte, R. Hackert, W. Ilg, J. Biltzinger, N. Schilling, F. Biedermann, M. Jergas, H. Preuschoft and M. S. Fischer, "Quadrupedal Mammals as Paragons for Walking Machines," in *Proceeding of the International Symposium on Adaptive Motion in Animals and Machines (AMAM)*, Montreal, 2000.

[49] M. Fischer and R. Blickhan, "The tri-segmented limbs of therian mammals: kinematics, dynamics, and self-stabilization. A review.," in *Journal of Experiemnatl Zoology 305A*, 2006.

[50] S. Rutishauser, "Cheetah - compliant quadruped robot," École Polytechnique Fédérale de Lausanne, Lausanne, 2008.

[51] R. Blickhan, A. Seyfarth, H. Geyer, S. Grimmer, H. Wagner and M. Günther, "Intelligence by mechanics," *Phil. Trans. The Royal Society,* vol. 365, p. 199–220, 2007.

[52] J. Rummel and A. Seyfarth, "Stable Running with Segmented Legs," *Manuscript: The International Journal of Robotics Research,* vol. 27, pp. 919-934, 2008.

[53] A. Tuleu, "Trot Gait Locomotion of a Cat Sized Quadruped Robot," Switzerland, 2009.

[54] A. Seyfarth, H. Geyer, S. Lipfert, J. Rummel, Y. Minekawa and F. Iida, "Running and walking with compliant legs," *Fast Motions in Biomechanics and Robotics: Optimization and Feedback Control,* p. 383–402, 2006.

[55] A. Tuleu, "Improvement of the Cheetah Locomotion Control," École Polytechnique Fédérale de Lausanne, Lausanne, Switzerland, 2010.

[56] C. T. Farley, J. Glasheen and T. A. McMahon, "Running springs: speed and animal size," *Journal of experimental Biol.,* p. 185: 71–86, 1993.

[57] L. Küchler, "Segmented Leg Design in Robotics," Biologically Inspired Robotics Group - Master thesis, 2010.

[58] A. Spröwitz, S. Rutishauser and A. Jan Ijspeert, "Compliant quadruped robot cheetah passive and active leg mechanics," Biologically Inspired Robotics Group, EPFL, Switzerland, 2009.

[59] A. Seyfarth, "A movement criterion for running," *Journal of Biomechanics,* 2002.

[60] A. Seyfarth, H. Geyer and H. Herr, "Swing-leg retraction: a simple control model for stable running," *The Journal of Experimental Biology,* vol. 206, pp. 2547-2555, 2003.

[61] G. Brambilla, J. Buchli and A. Jan Ijspeert, "Adaptive Four Legged Locomotion Control Based on Nonlinear Dynamical Systems," in *Proceedings of The Ninth International Conference on*

the SIMULATION OF ADAPTIVE BEHAVIOR, 2006.

[62] C. F. Beards, Structural Vibration: Analysis and Damping, Arnold, 1996.

[63] H. A. Rothbart, Mechanical design handbook: measurement, analysis, and control of dynamic systems, McGraw-Hill Handbooks, 2006.

[64] J. Prentis, Dynamics of mechanical systems, E. Horwood, 1980.

[65] Webots Reference Manual, vol. 6.3.4, Switzerland: Cyberbotics Ltd., 2011.

[66] M. R. Fielding, C. J. Damaren and R. Dunlop, "Hamlet: Force/Position Controlled Hexapod Walker - Design and Systems," in *Proc. IEEE Int Conf of Controll Appl Mexico*, 2001.

[67] M. Hutter, C. D. Remy and R. Siegwart, "Design of an Articulated Robotic Leg with Nonlinear Series Elastic Actuation," in *Proc. of The 12th International Conference on Climbing and Walking Robots and the Support Technologies for Mobile Machines (CLAWAR)*, 2009.

[68] M. Hutter, C. D. Remy, M. A. Hoepflinger and R. Siegwart, "High Compliant Series Elastic Actuation For The Robotic Leg Scarleth," in *Proc. of the International Conference on Climbing and Walking Robots (CLAWAR)*, 2011.

Appendixes

A. Webots™ world file

Next is presented the world file developed in Webots™ for the left front leg. The same patter was reproduced for the remaining quadruped walking members.

FRONT_LEFT_1_SERVO Servo

Rotation		0	0	1	-0,4963
Name		"front_left_1"			
Physics					
	Density	-1			
	Mass	0,012			
	Center of mass	-0,006	-0,003	0	
	(...)				
	Coloumb friction	0,995			
	Force dependent slip	0,005			
Type		rotational			
Max velocity		*5,34008*			
Max force		*16181*			
(...)					
Position		0			
minPosition		0			

maxPosition 0

minStop 0

maxStop 0

spring constant 0

damping constant 0

F1_FRONT_LEFT_1_TRANS Trans { F1_SHAPE Shape }

FRONT_LEFT_2_SERVO Servo

Rotation 1 0 0 1,5708

Name “front_left_2”

Physics

Density -1

Mass 0,126

Center of mass -0,002 -0,002 0,0415

(...)

Coloumb friction 0,995

Force dependent 0,005

p

Type rotational

Max velocity *5,34008*

Max force *16181*

(...)

Position 1,5708

minPosition 0

maxPosition 0

minStop 0

maxStop 0

spring constant 0

damping constant 0

AX12_FRONT_LEFT_2_TRANS Trans { AX12_SHAPE }

F3_FRONT_LEFT_3_TRANS

FRONT_LEFT_3_E Servo

Translation 0 0 0,083

Rotation 0 1 0 0,8727

Name “front_left_3”

Physics

Density -1

Mass 0,058

Center of mass 0 0 0,035

	(...)				
	Coloumb friction	0,995			
	Force dependent slip	0,005			
Type		rotational			
Max velocity		*5,34008*			
Max force		*10*	16181		
(...)					
Position		0			
minPosition		0			
maxPosition		0			
minStop		0			
maxStop		0			
spring constant		0			
damping constant		0			
F3_FRONT_LEFT_L2 Trans {L2 SHAPE}					
FRONT_LEFT_3_F Servo					
Translation		0	0	0,057	
Rotation		0	1	0	0,8727
Name		“front_left_3p”			
Physics					
	Density	-1			
	Mass	0,058			
	Center of mass	0	0	0,035	
	(...)				
	Coloumb friction	0,995			
	Force dependent slip	0,005			
Type		rotational			
Max velocity		*5,34008*			
Max force		*0*			
(...)					
Position		0			
minPosition		0			
maxPosition		0			
minStop		0			
maxStop		0			
spring constant		0			
damping constant		0			
F3_FRONT_LEFT_L4 Trans {L4 SHAPE}					
FRONT_LEFT_4_D Servo					
Translation		0	0	0,07	
Rotation		0	1	0	-0,8727
Name		“front_left_4”			
Physics					

	Density	-1		
	Mass	0,069		
	Center of mass	0	0	0,0415
	(...)			
	Coloumb friction	0,995		
	Force dependent slip	0,005		
Type		rotational		
Max velocity		*5,34008*		
Max force		*0*		
(...)				
Position		0		
minPosition		0		
maxPosition		0		
minStop		0		
maxStop		0		
spring constant		1,5		
damping constant		0,01		

B. Physics plug-in input

```
#include <ode/ode.h>
#include <plugins/physics.h>

dJointID FL_L2_L1;
dJointID FR_L2_L1;
dJointID BL_L2_L1;
dJointID BR_L2_L1;

void webots_physics_init(dWorldID world, dSpaceID space, dJointGroupID contactJointGroup) {

//FRONT LEFT C joint
dBodyID FL_L1 = dWebotsGetBodyFromDEF("FRONT_LEFT_4_D");
if (!FL_L1) return;
dBodyID FL_L2 = dWebotsGetBodyFromDEF("FRONT_LEFT_3_E");
if (! FL_L2) return;


FL_L2_L1  = dJointCreateHinge(world, 0);
dJointAttach(FL_L2_L1, FL_L1, FL_L2);

  dVector3 point_C_FL;
  dBodyGetRelPointPos (FL_L2, 0,0,0.035, point_C_FL);

  dJointSetHingeAnchor (FL_L2_L1, point_C_FL[0], point_C_FL[1],point_C_FL[2]);

  dJointSetHingeAxis (FL_L2_L1, 0, 0,1);
```

```
//FRONT RIGHT C joint
dBodyID FR_L1 = dWebotsGetBodyFromDEF("FRONT_RIGHT_4_D");
if (!FR_L1) return;
dBodyID FR_L2 = dWebotsGetBodyFromDEF("FRONT_RIGHT_3_E");
if (! FR_L2) return;

FR_L2_L1  = dJointCreateHinge(world, 0);
dJointAttach(FR_L2_L1, FR_L1, FR_L2);

 dVector3 point_C_FR;
 dBodyGetRelPointPos (FR_L2, 0, 0, 0.035,point_C_FR);

 dJointSetHingeAnchor (FR_L2_L1, point_C_FR[0], point_C_FR[1],point_C_FR[2]);

 dJointSetHingeAxis (FR_L2_L1, 0, 0,1);

//BACK LEFT C joint
dBodyID BL_L1 = dWebotsGetBodyFromDEF("BACK_LEFT_4_D");
if (!BL_L1) return;
dBodyID BL_L2 = dWebotsGetBodyFromDEF("BACK_LEFT_3_E");
if (! BL_L2) return;

BL_L2_L1  = dJointCreateHinge(world, 0);
dJointAttach(BL_L2_L1, BL_L1, BL_L2);

 dVector3 point_C_BL;
 dBodyGetRelPointPos (BL_L2, 0, 0, 0.035,point_C_BL);

 dJointSetHingeAnchor (BL_L2_L1, point_C_BL[0], point_C_BL[1],point_C_BL[2]);

 dJointSetHingeAxis (BL_L2_L1, 0, 0,1);

//BACK RIGHT C joint
dBodyID BR_L1 = dWebotsGetBodyFromDEF("BACK_RIGHT_4_D");
if (!BR_L1) return;
dBodyID BR_L2 = dWebotsGetBodyFromDEF("BACK_RIGHT_3_E");
if (! BR_L2) return;

BR_L2_L1  = dJointCreateHinge(world, 0);
dJointAttach(BR_L2_L1, BR_L1, BR_L2);

 dVector3 point_C_BR;
 dBodyGetRelPointPos (BR_L2, 0, 0, 0.035,point_C_BR);

 dJointSetHingeAnchor (BR_L2_L1, point_C_BR[0], point_C_BR[1],point_C_BR[2]);

 dJointSetHingeAxis (BR_L2_L1, 0, 0,1);
```

C. AX-12 servo dimensions

The servomotor presents a compact size whose dimensions are a fundamental to the design and segmentation dimensioning of the robots leg [6]:

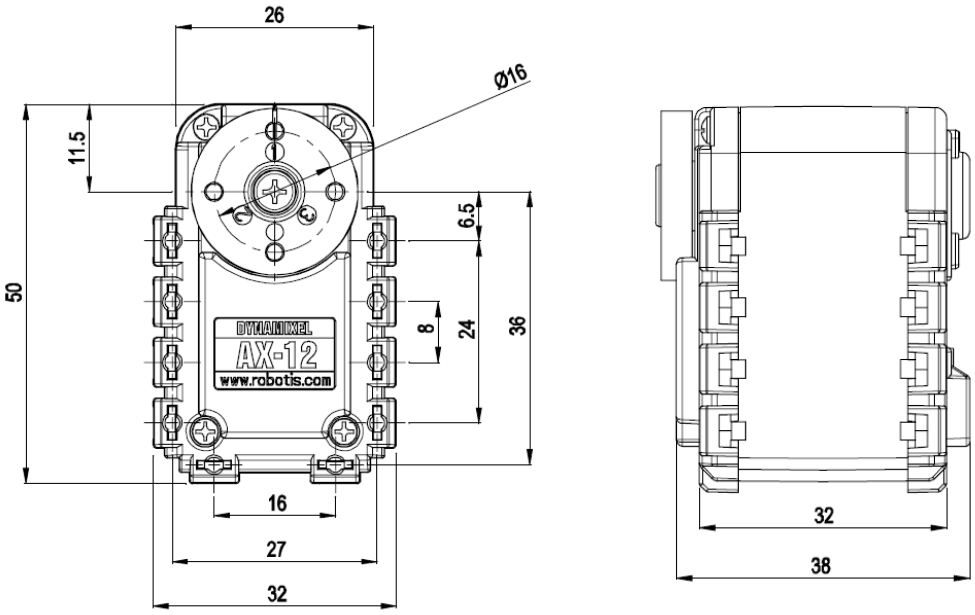

Figure C.1 - Servo AX-12 schematic dimensions (mm) [6]

D. Controller main command

```
void BioloidQuadRobot::run() {
        init();
        while(step(SIMULATION_STEP)!=-1){
                getJointValues();

// dynamical system computations
                myCPG.integrate(h,h);
                t += h;
                for(int i=0;i<NB_States;i++)
                        state[i]=myCPG.getState(i)->getValue();

                // get the angles theta from x states
```

```
                theta[Front_Left][HipPitch] = state[x_Front_Left_HipPitch];
                theta[Front_Right][HipPitch] = state[x_Front_Right_HipPitch];
                theta[Back_Left][HipPitch] = state[x_Back_Left_HipPitch];
                theta[Back_Right][HipPitch] = state[x_Back_Right_HipPitch];

    if(state[z_Front_Left_HipPitch]<0) { //swing
      joint[Front_Left][Knee]->setPosition(deg2rad(theta[Front_Left][Knee]));
            } else{
                joint[Front_Left][Knee]->setForce(0);
              }

               if(state[z_Front_Right_HipPitch]<0) {
      joint[Front_Right][Knee]->setPosition(deg2rad(theta[Front_Right][Knee]));
    } else{
                joint[Front_Right][Knee]->setForce(0);
              }

    if(state[z_Back_Left_HipPitch]<0) {
      joint[Back_Left][Knee]->setPosition(deg2rad(theta[Back_Left][Knee]));
    } else{
                joint[Back_Left][Knee]->setForce(0);
              }
    if(state[z_Back_Right_HipPitch]<0) {
      joint[Back_Right][Knee]->setPosition(deg2rad(theta[Back_Right][Knee]));
    } else{
                joint[Back_Right][Knee]->setForce(0);
              }


    joint[Front_Left][HipPitch]->setPosition(deg2rad(theta[Front_Left][HipPitch]));
    joint[Front_Right][HipPitch]->setPosition(deg2rad(theta[Front_Right][HipPitch]));
    joint[Back_Left][HipPitch]->setPosition(deg2rad(theta[Back_Left][HipPitch]));
    joint[Back_Right][HipPitch]->setPosition(deg2rad(theta[Back_Right][HipPitch]));

                write2file();
      }
      write2fileobj.writebuffer2file(".//WebotsExperiment/exp.dat");
}

void BioloidQuadRobot::init() {
```

```
        for(int i = omega_Front_Left_HipPitch; i<=omega_Back_Right_HipPitch; i++)
                myParameters[i] = -2*pi/.7;

        for(int i = mu_Front_Left_HipPitch; i<=mu_Back_Right_HipPitch; i++)
                myParameters[i] = 20*20; //alteração da amplitude da hip
                for(int i = b_Front_Left_HipPitch; i<=b_Back_Right_HipPitch; i++)
                myParameters[i] = 500;

        myParameters[relosc] = 0.1;
        for(int i = alpha_Front_Left_HipPitch; i<=alpha_Back_Right_HipPitch; i++)
                myParameters[i] = 1/abs(2*myParameters[mu_Front_Left_HipPitch+i-
alpha_Front_Left_HipPitch]*myParameters[relosc]);

        myParameters[offset_Front_Left_HipPitch] = 0;
        myParameters[offset_Front_Right_HipPitch] = 0;
        myParameters[offset_Back_Left_HipPitch] = -0;
        myParameters[offset_Back_Right_HipPitch] = -0;

// set initial joint values
        theta[Front_Left][HipPitch] = myParameters[offset_Front_Left_HipPitch];
        theta[Front_Left][HipFlap] = 90;
        theta[Front_Left][Knee] = 0; //alteração do valor inicial do joelho para 0
        theta[Front_Right][HipPitch] = myParameters[offset_Front_Right_HipPitch];
        theta[Front_Right][HipFlap] = -90;
        theta[Front_Right][Knee] = 0;
        theta[Back_Left][HipPitch] = myParameters[offset_Back_Left_HipPitch];
        theta[Back_Left][HipFlap] = 90;
        theta[Back_Left][Knee] = 0;
        theta[Back_Right][HipPitch] = myParameters[offset_Back_Right_HipPitch];
        theta[Back_Right][HipFlap] = -90;
        theta[Back_Right][Knee] = 0;

        theta_neck_1 = -90;
        theta_neck_2 = 0;
        theta_head = 0;
        theta_pelvis = 0;
        setJointValues();
        // wait 2 seconds before carrying on;
        for(int i=0; i<((int)2/(SIMULATION_STEP*0.001)); i++) {
                step(SIMULATION_STEP);
        }
```

```
        theta[Front_Left][Knee] = 50;
        theta[Front_Right][Knee] = 50;
        theta[Back_Left][Knee] = 50;
        theta[Back_Right][Knee] = 50;

// Simulation parameters and system states
        t = 0;
        // dynamical system
        myParameters[h_step] =SIMULATION_STEP *  0.001;
        h = myParameters[h_step];

        // set initial dynamical states
        state[x_Front_Left_HipPitch] = sqrt(myParameters[mu_Front_Left_HipPitch]);
        state[x_Front_Right_HipPitch] = -state[x_Front_Left_HipPitch];
        state[x_Back_Left_HipPitch] = -state[x_Front_Left_HipPitch];
        state[x_Back_Right_HipPitch] = state[x_Front_Left_HipPitch];

        state[z_Front_Left_HipPitch] = 0.01;
        state[z_Front_Right_HipPitch] = -0.01;
        state[z_Back_Left_HipPitch] = 0.01;
        state[z_Back_Right_HipPitch] = -0.01;

        // assign states and parameters
        myCPG.setParameters(myParameters);
   myCPG.setStates(state);

// write to file buffer
        write2fileobj.CreateBuffer(21,100000);
}
```

E. Simulation Graphics

Simulation trajectory of the leg knee angle variation during simulation, comparing the theoretical values expected with the Webots™ simulation values for the different damping constants when the spring constant is fixed to spring values:

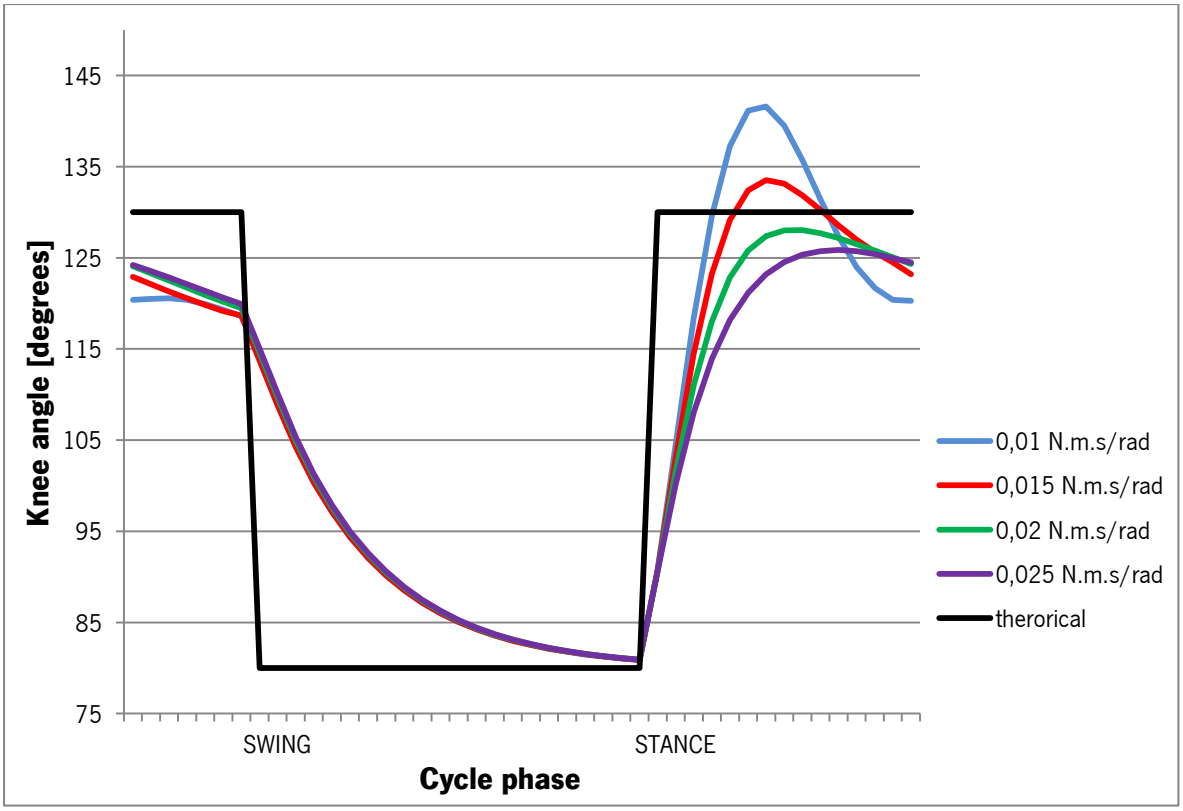

Figure E.1 - Simulation trajectory of the theoretical (black line) and practical knee angles during the step cycle with spring constant of 0.5 N.m/rad for different damping constant values.

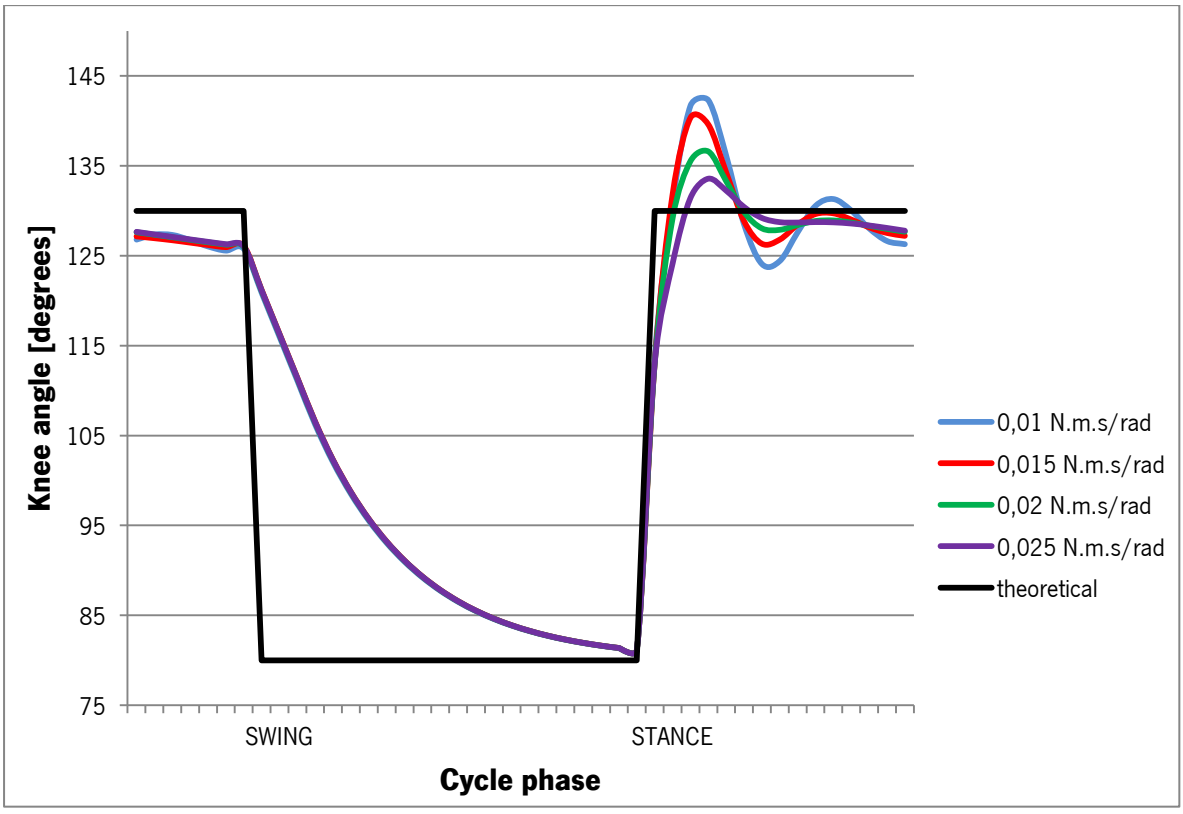

Figure E.2 – Simulation trajectory of the theoretical (black line) and practical knee angles during the step cycle with spring constant of 1.5 N.m/rad for different damping constant values.

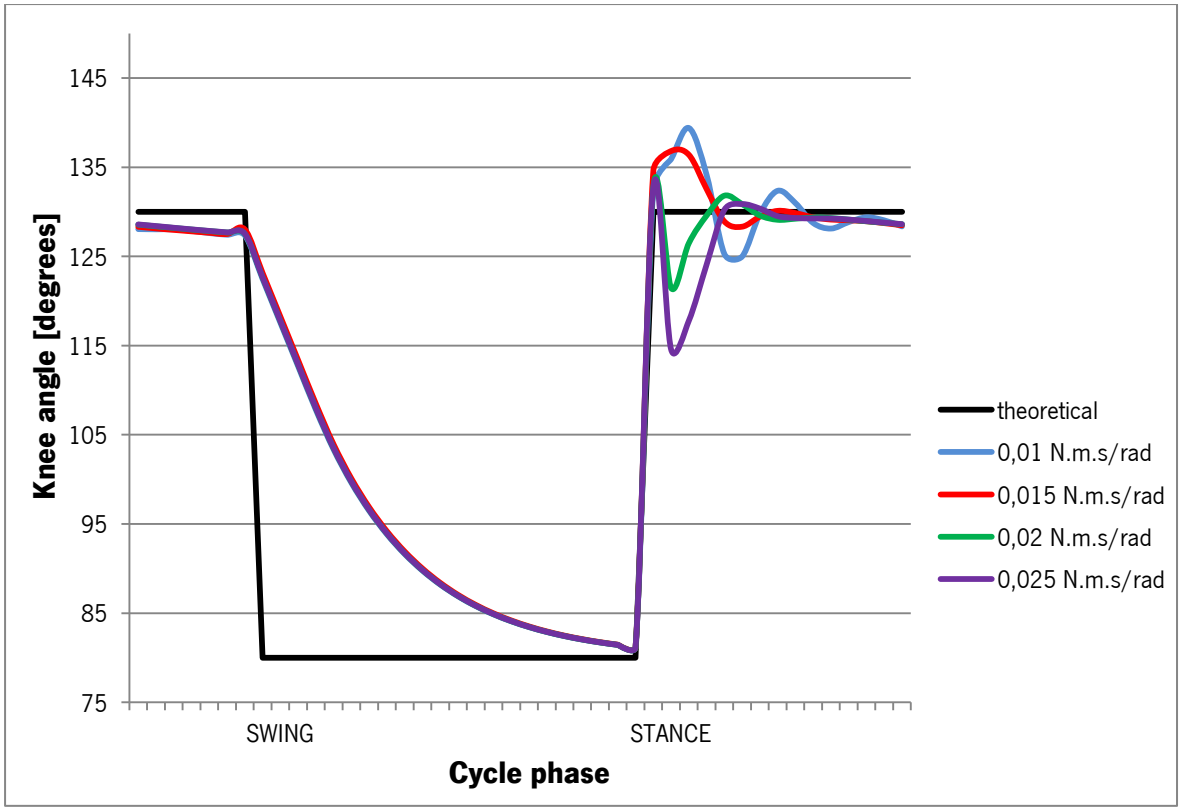

Figure E.3 - Simulation trajectory of the theoretical (black line) and practical knee angles during the step cycle with spring constant of 2.0 N.m/rad for different damping constant values.

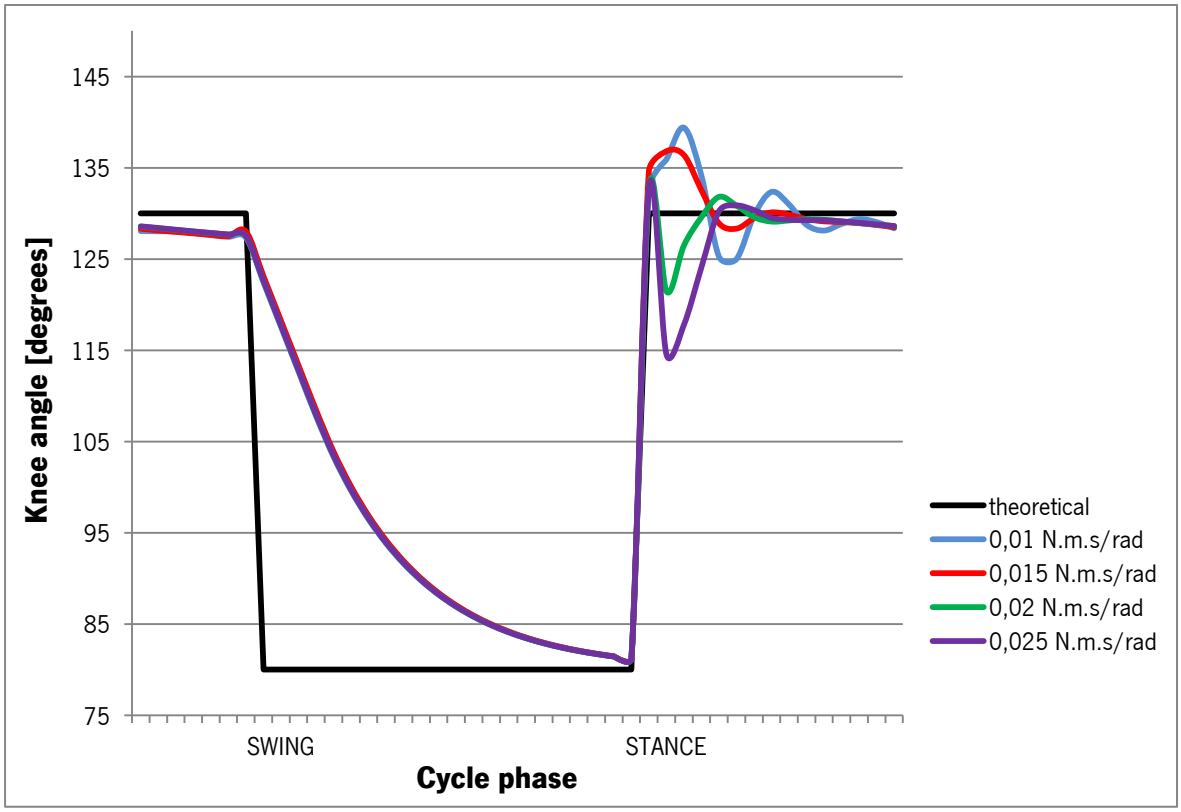

Figure E.4 - Simulation trajectory of the theoretical (black line) and practical knee angles during the step cycle with spring constant of 2.5 N.m/rad for different damping constant values.

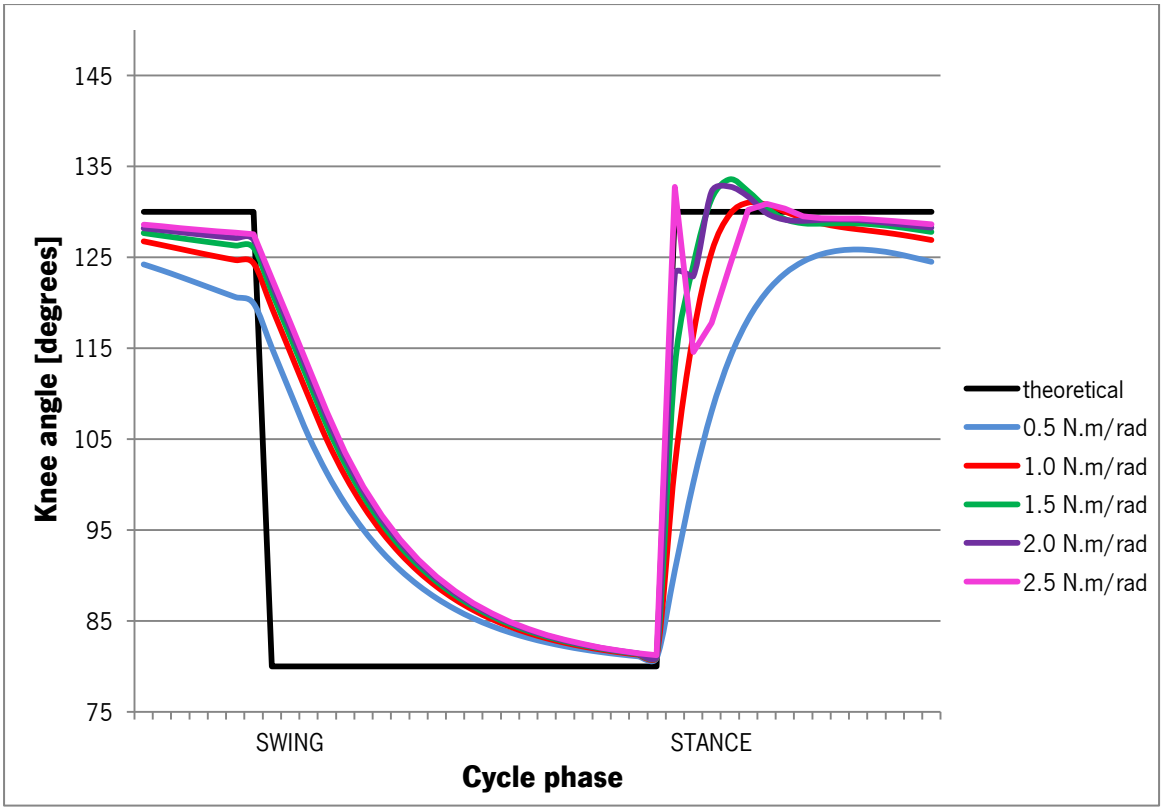

Figure E.5 - Simulation trajectory of the theoretical (black line) and practical knee angles during the step cycle with damping constant of 0.015 N.m.s/rad for different spring constant values.

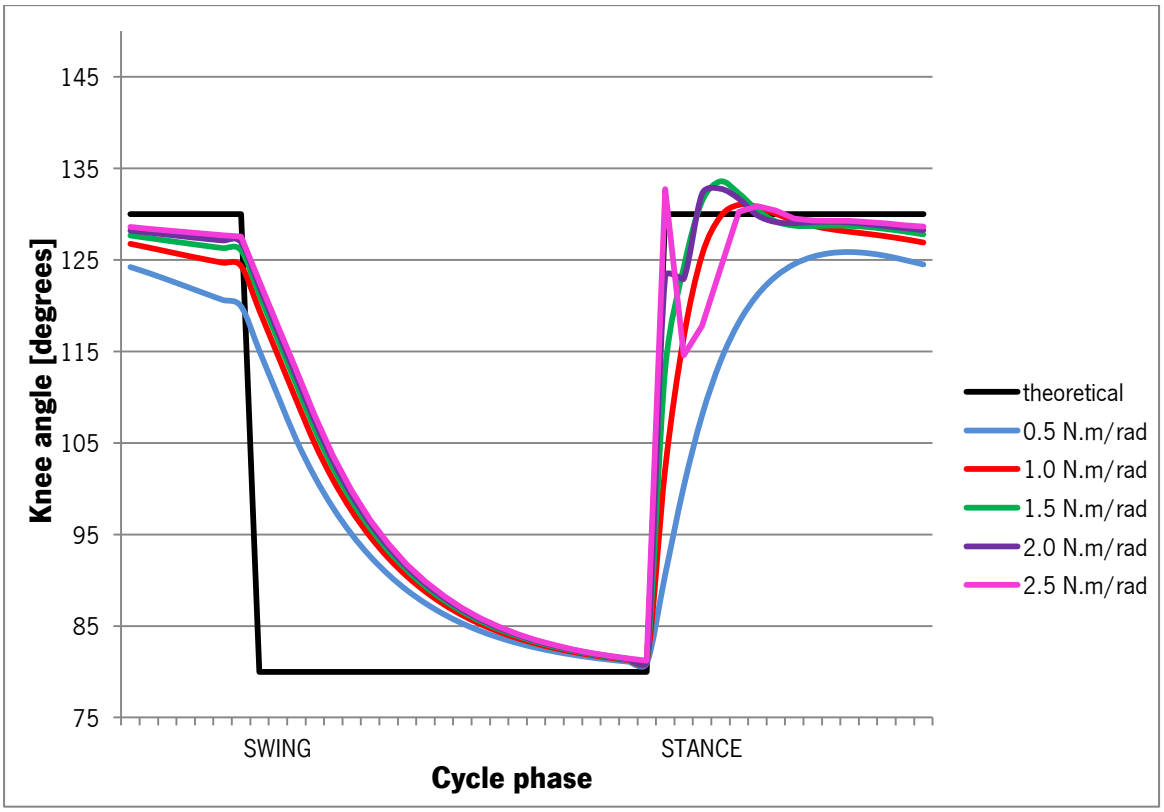

Figure E.6 - Simulation trajectory of the theoretical (black line) and practical knee angles during the step cycle with damping constant of 0.025 N.m.s/rad for different spring constant values